BIOMATERIALS

Sprayable extracellular matrix hydrogel reduces postoperative adhesion formation and protects healing tissues in preclinical models

Lucía Pascual-Antón[1]†, Pilar Sandoval[1]†*, Henar Tomero-Sanz[1], Michela Terri[2,3,4], Raffaele Strippoli[2,3,4], Íñigo García-Sanz[5], Cristina Marín-Campos[5], Miguel Ángel del Pozo[2], Maryam Obaid[6], Valentina Garcia[6], Peter Alex Smith[6], Timothy J. Keane[6,7], Molly M. Stevens[7,8]*, Manuel López-Cabrera[1]*

Tissue trauma initiates inflammation that can lead to fibrotic complications such as postoperative peritoneal adhesions, which contribute to chronic pain, infertility, and bowel obstruction. Despite their prevalence and impact, effective interventions to prevent adhesion formation remain limited. In this study, we evaluated a sprayable extracellular matrix (ECM) hydrogel as a barrier to protect healing tissues and reduce adhesion formation after abdominal surgery. In both mouse and rabbit models of colorectal and gynecologic procedures, ECM hydrogel application resulted in a substantial reduction in adhesion severity. Mechanistic studies demonstrated that the hydrogel promotes preservation or restoration of the mesothelial lining while modulating early local inflammation. Treated tissues exhibited reduced expression of inflammatory cytokines, including IL-1β, and maintained an intact mesothelial surface with fewer activated myofibroblasts compared with synthetic hydrogel and controls. Immunohistochemical analysis, transcriptomic profiling of mesothelial cells, and in vitro mechanical stretch experiments revealed that the ECM hydrogel mitigates mesothelial-to-mesenchymal transition. These findings suggest that the hydrogel not only provides a physical barrier but also serves as a biological modulator, shielding tissue from mechanical and inflammatory cues that drive adhesion formation. Overall, this study identifies a dual-function, biologically active ECM hydrogel capable of protecting healing tissues and reducing adhesion development in preclinical surgical models. These results support the potential of ECM hydrogel as a clinically translatable, biocompatible strategy for improving postsurgical healing outcomes and reducing adhesion-related complications.

INTRODUCTION

Postsurgical peritoneal adhesions (PAs) are fibrous connective tissue bands that commonly form in response to trauma or surgical procedures that involve the peritoneal cavity (*1*). PAs inappropriately attach abdominal organs to the parietal peritoneal surface or to another organ (*2*, *3*). Although good surgical technique can limit excessive peritoneal damage, more than 93% of patients undergoing laparotomy will experience complications associated with PAs (*4*). PAs can also lead to deleterious outcomes in patients months or years after surgery, posing a lasting burden on the health care system. Patients with PAs may face infertility (*5*), chronic abdominal pain, intestinal obstruction, and even death. In the case of secondary surgeries, PAs can prolong surgical duration, extend time under anesthesia, and increase health costs (*6*, *7*).

[1]Tissue and Organ Homeostasis Program, Centro de Biología Molecular Severo Ochoa (CBM), CSIC, Universidad Autónoma de Madrid, 28049 Madrid, Spain. [2]Mechanoadaptation and Caveolae Biology Laboratory, Area of Cell and Developmental Biology, Centro Nacional de Investigaciones Cardiovasculares (CNIC), 28029 Madrid, Spain. [3]Department of Molecular Medicine, Sapienza University of Rome, 00161 Rome, Italy. [4]Gene Expression Laboratory, National Institute for Infectious Diseases, Lazzaro Spallanzani IRCCS, 00149 Rome, Italy. [5]Department of General and Digestive Surgery, Hospital Universitario La Princesa–Instituto de Investigación Sanitaria Princesa (IIS-IP), Universidad Autónoma de Madrid, 28006 Madrid, Spain. [6]TYBR Health Inc. Houston, TX 77021, USA. [7]Department of Materials, Department of Bioengineering, Institute of Biomedical Engineering, Imperial College London, SW7 2AZ London, UK. [8]Kavli Institute for Nanoscience Discovery, Department of Physiology, Anatomy and Genetics, Department of Engineering Science, University of Oxford, OX1 3QU Oxford, UK.
†These authors contributed equally to this work.
*Corresponding author. Email: psandoval@cbm.csic.es (P.S.); molly.stevens@dpag.ox.ac.uk (M.M.S.); mlcabrera@cbm.csic.es (M.L.-C.)

The formation of adhesions after abdominal surgery has been described as a sequential process that begins with uncontrolled recruitment of a resident population of macrophages from the peritoneal cavity to the site of damage (*8*). These macrophages shift the balance between coagulation and fibrinolysis toward the coagulation system, which leads to deposition of a fibrin scaffold and subsequent ingrowth of fibrotic tissue (*9*). Last, PAs can become sensitive to pain after possible ingrowth of blood vessels and nerves (*6*, *10*).

A monolayer of mesothelial cells (MCs) lines most of the organs housed in the peritoneal cavity and the entire cavity wall. These MCs have antiadhesive properties, which act as the first barrier protecting most intra-abdominal organs against microorganisms and invading tumor cells (*11*–*13*). We previously demonstrated that MCs play a key role in PA development, through their conversion into myofibroblasts by a mesothelial-to-mesenchymal transition (MMT) process (*14*). During MMT, MCs acquire migratory and invasive capacities, increase extracellular matrix (ECM) production, and transdifferentiate into active myofibroblasts (*14*–*18*). In healthy peritoneum, podoplanin (PDPN) expression is restricted to MCs and lymphatic endothelium (*19*). In damaged peritoneum, PDPN is expressed in myofibroblasts derived from MCs (*20*), thus providing a lineage handle that we exploit throughout this study. Recent studies suggest that MMT induced by acute peritoneal damage, such as that occurring during surgery-related trauma, is a determinant triggering factor in the pathogenesis of PAs. Specifically, exposure of the peritoneum to surgery-related mechanical forces induces a robust MMT response, which involves cooperation between biomechanical pathways and biochemical signaling mediators such as

transforming growth factor–β1 (TGF-β1). The proportional contribution of the mechanical forces and biochemical factors, respectively, to MMT depends on the extent of peritoneal injury involved and whether the injury is acute or chronic (*21*, *22*).

The past 20 years have seen development and testing of multiple strategies to protect against PAs, including pharmacological agents and physical barriers such as gels or films, but all have limited clinical efficacy (*6*, *23*–*26*). Pharmaceutical agents lack longevity at the surgically injured site (*6*, *24*, *27*), and physical barriers, such as films or sheets, are difficult to handle and apply (*23*, *28*–*31*). The requirements of an ideal tissue protector material include (i) being injectable or easily applied by surgeons without the need for sutures or staples, (ii) being biocompatible. and (iii) remaining in place during the critical initial phase of tissue healing and regeneration until remesothelization occurs (*6*, *23*). Hydrogels are a promising therapeutic strategy capable of meeting these requirements. Compared with alternative barrier materials, hydrogels offer increased retention time and better coverage of the injured tissue (*32*, *33*). Moreover, ECM-based hydrogels have been safely and effectively used in numerous preclinical and clinical applications for tissue repair (*34*–*36*).

We developed an ECM hydrogel obtained through decellularization of porcine bone tissue. This ECM hydrogel is thermosensitive and exhibits intermediate solid-liquid properties. Below 22°C, it is a liquid with low viscosity, allowing it to be easily applied as a spray. When it is heated to 30° to 37°C, it quickly forms a gel, allowing gelation at the site of application. Because of this viscoelastic behavior, the ECM hydrogel maintains the separation of tissues while enabling the intraperitoneal mobility of the visceral organs.

In this study, we evaluated the effect of our ECM hydrogel barrier on the formation of postoperative PAs. MCs treated with the ECM hydrogel showed a modulated MMT-associated response to mechanical stretch in vitro, and tissues preserved mesothelial integrity in vivo. Compared with controls, hydrogel-treated tissues exhibited reduced local production of proinflammatory cytokines, maintenance of an intact mesothelial lining, and decreased chronic inflammatory responses. Applying the ECM hydrogel to surgically injured peritoneal tissues thereby led to a reduction in the incidence and severity of adhesions in murine and rabbit models of colorectal and gynecological surgery, respectively.

RESULTS

RNA sequencing analyses of MCs derived from PAs reveal a mechanically induced MMT signature

To compare the gene expression profile of control MCs compared with PA-associated cells, we first isolated and characterized peritoneal cells sorted for $PDPN^+/CD45^-$ from human clinical samples obtained from omentum and postsurgical PAs (Fig. 1, A to D) or mouse samples obtained from the peritoneal cavity and PAs induced after 5 days in mice undergoing an ischemic button (IB)–based surgery model (Fig. 1, E to H). PDPN, which is highly expressed on MCs, was used to identify MCs and MC-derived cells (*20*). CD45 was used to exclude any cells of hematopoietic origin such as macrophages that may respond to the peritoneal injury (*31*). PDPN is expressed in MCs and lymphatic endothelium (*19*) and has also been described in MMT-related peritoneal diseases, such as fibrosis associated with peritoneal dialysis (*37*), encapsulating peritoneal sclerosis (*38*, *39*), peritoneal metastasis (*40*), or PAs (*20*, *31*). Morphologically, cells isolated from PAs in both human (HPAMCs) and mouse (MPAMCs) showed an elongated shape characteristic of fibroblasts, in contrast with the cobbled morphology of control human (HPMCs) and mouse (MPMCs) peritoneal MCs (Fig. 1, A and E). Flow cytometry analysis of $PDPN^+$ control HPMCs was largely negative for fibroblast activation protein (FAP) expression (fig. S1A), indicating the absence of activated resident fibroblasts in the control MCs. In the $PDPN^+$ cells from human PAs, more than 98% of the culture coexpressed PDPN and FAP (fig. S1B), which indicates a transition to a more activated fibroblastic phenotype in PA-derived cells. To further validate the identity of the $PDPN^+/CD45^-$ cells, we evaluated the expression of several mesothelial and mesenchymal immunohistochemical markers in human control peritoneal tissue. The control mesothelial monolayer was positive for PDPN and cytokeratin (CK) but did not express α–smooth muscle actin (α-SMA) (fig. S2A). In healthy control tissue, α-SMA was limited to a few capillaries in the submesothelial zone, where there are not FAP^+ cells, indicative of activated fibroblasts. Immunohistochemistry of PA biopsies from patients undergoing laparotomy revealed large areas of staining for MC markers (PDPN and CK) within the adhesion tissue. In serial sections, the tissue stained with MC markers also expressed mesenchymal markers (α-SMA and FAP) (fig. S2B). Consistent with prior literature (*14*, *20*, *21*), these findings support a conversion of MCs into activated myofibroblasts within adhesion tissue, although other minority populations of fibroblasts could also contribute to adhesion fibrosis.

Using these $PDPN^+/CD45^-$ cells isolated from human clinical samples or mouse peritoneal samples, we performed two independent RNA sequencing (RNA-seq) studies. Bulk RNA-seq of human $PDPN^+/CD45^-$ cultures yielded a distinct separation between PA-isolated MCs and control MCs in a clustered heatmap (Fig. 1B) and by principal components analysis (fig. S3A). In HPAMCs, there were a total of 2869 differentially expressed genes (DEGs) ($P < 0.05$) (1572 up-regulated and 1297 repressed) as compared with HPMCs (fig. S3B). Parallel evaluation of mouse MCs showed a similar transcriptomic separation in MPAMCs, with 3506 DEGs ($P < 0.05$) (1476 up-regulated and 2030 repressed) as compared with MPMCs (Fig. 1F and fig. S4, A and B). Pathway analysis indicated enrichment of several canonical signaling pathways associated with adhesion formation mechanisms, such as epithelial-to-mesenchymal transition (EMT), hypoxia, wound healing, vascularization, and coagulation in HPAMCs (Fig. 1C and data file S1). Many adhesion-related pathways were also enriched in MPAMCs (Fig. 1G and data file S1). In both human and mouse PA–associated $PDPN^+$ cells, we also identified an enrichment in mechanical MMT-related signaling pathways, including Hippo signaling and caveolar-mediated signaling (Fig. 1, C and G).

Detailed analyses of DEGs in both human and murine cells revealed a significant ($P < 0.05$) repression of typical mesothelial markers in $PDPN^+/CD45^-$ cells from PA tissues, including *Wilms' tumor gene 1* (*WT1*), CKs (*KRTs*), and claudins, as well as up-regulation of mesenchymal markers such as collagens, *fibronectin 1* (*FN1*), *matrix metalloproteinases* (*MMP*s), and fibroblast markers [*FAP*, *fibroblast-specific protein-1* (*FSP-1*/*S100A4*) and *actin α2, smooth muscle* (*ACTA2*/*α-SMA*)]. The $PDPN^+/CD45^-$ cells from healthy tissue were consistent with mesothelium, whereas the $PDPN^+/CD45^-$ cells isolated from PA tissues adopted a more fibroblastic gene expression profile, consistent with the process of MMT. We also found up-regulation of genes closely related to MMT biochemical signaling in the PA-associated cells, which were mainly related to TGF-β

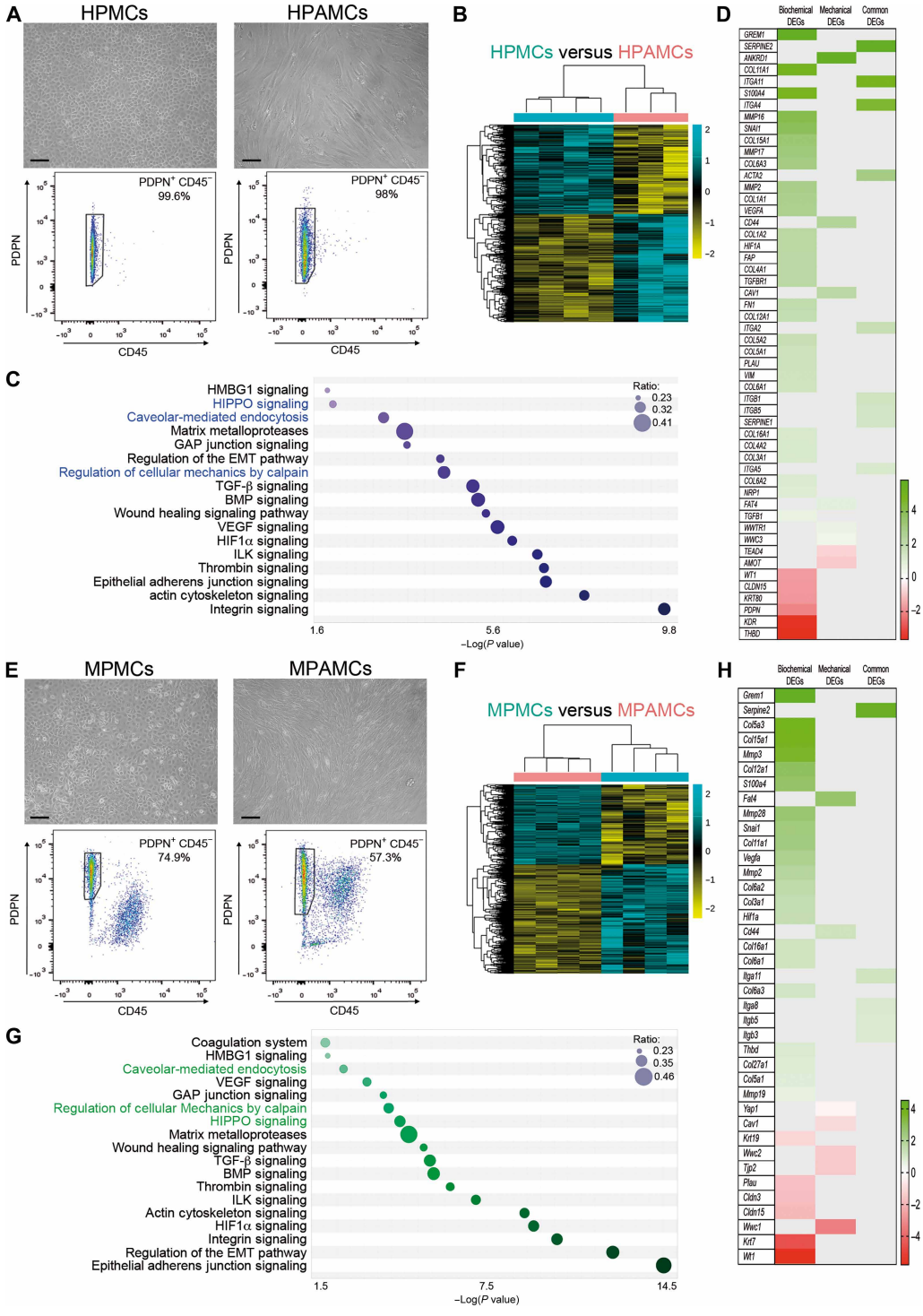

Fig. 1. RNA-seq analyses of human and mouse PA–isolated MCs. (**A**) Representative images of control HPMCs (top left) and fibroblast-like cells isolated from a patient with a PA (top right). Scale bars, 100 μm. Flow scatterplots of FACS-isolated $CD45^-/PDPN^+$ cells (bottom) for RNA-seq analysis. (**B**) Heatmap representing DEGs in HPAMCs of patients with PA ($n = 3$) as compared with control HPMCs ($n = 4$). (**C**) Bubble chart showing differentially regulated canonical pathways in HPAMCs analyzed with Ingenuity Pathway Analysis (IPA) software. Mechanical canonical pathways are presented in blue. (**D**) Heatmap representing significant differentially expressed MMT-related genes separated into biochemical, mechanical, and shared pathways. (**E**) Representative images of control MPMCs (top left) and fibroblast-like MPAMCs isolated from the IB mouse model (top right). Scale bars, 100 μm. Scatterplot of $CD45^-/PDPN^+$ cells isolated by FACS (bottom). (**F**) Heatmap representing DEGs in MPAMCs ($n = 4$) as compared with control MPMCs ($n = 4$). (**G**) Significant differentially regulated canonical pathways in MPAMCs analyzed with IPA software. Mechanical signaling pathways are highlighted in green. (**H**) Heatmap representing significant DEGs associated with MMT and separated in biochemical, mechanical, and shared pathways. Heatmaps in (B) and (F) were generated using hierarchical clustering based on Euclidean distances between samples, with the complete linkage method (default in the R function hclust). In (C) and (G), the *x* axis indicates statistical significance [−log (*P* value) > 1.3], calculated using the Benjamini-Hochberg correction. Color intensity of bubbles represents −log (*P* value). Size of bubbles represents the ratio of overlapping genes to total genes in the pathway. The complete analysis with IPA software of differentially regulated canonical pathways in HPAMCs and MPAMCs is shown in data file S1. In (D) and (H), up-regulated, green; down-regulated, red; units, $\log_2$ fold change. Analysis by DESeq2 (https://bioconductor.org/packages/release/bioc/html/DESeq2.html), a R software package that calculates differential gene expression on the basis of the negative binomial distribution. $P < 0.05$ was considered statistically significant. HMBG1, high mobility group box 1; BMP, bone morphogenetic protein; ILK, integrin-linked kinase.

signaling, including *gremlin 1* (*GREM1*), TGF-β1 (*TGFB1*), *snail family transcriptional repressor 1* (*SNAI1*), and *MMP2*. In addition, DEGs closely related to mechanotransduction pathways were detected, including *ankyrin repeat domain 1* (*ANKDR1*), *CD44*, and *caveolin 1* (*CAV1*). Our results also showed significant ($P < 0.05$) DEGs, such as *plasminogen activator inhibitor 1* (*PAI-1/SERPINE1*) and integrins, which are shared by both biochemical and mechanical signaling pathways (Fig. 1, D and H). These results support cooperation between biochemical and biomechanical signals contributing to an MMT process in $PDPN^+$ cells in PAs. Moreover, the postsurgical PA mouse model reliably replicates most of the PA development process observed in patients.

Viscoelastic, tissue adherence, and proteomic properties of the ECM hydrogel

We next evaluated the flow properties of the ECM hydrogel material from decellularized porcine bone by steady-shear and step-shear rheology measurements, which are relevant to flow-based application processes such as spraying, spreading, or injection. The ECM hydrogel exhibited complete gelation within 2 min after neutralization and warming to physiological conditions (Fig. 2A). Gelation occurred through the assembly of collagen fibrils and physical entanglement, resulting in solidlike behavior (storage modulus greater than loss modulus) and largely linear viscoelastic responses up to strains of 100% in oscillatory rheological measurements (Fig. 2B). These results indicate that the ECM hydrogel preserves solidlike properties over an extremely broad range of strains. For reference, the highest strains experienced by tissues in the body are typically about 10% (*41*, *42*), which suggests that the ECM hydrogel material properties are likely to be maintained in the dynamic environment in the body.

The adherence of ECM hydrogel to model tissue was characterized using yield stress measurements. The yield behavior of the ECM hydrogel was equivalent for on-tissue and gel-only conditions (Fig. 2, C and D), indicative of a cohesive yielding behavior (failure of the gel itself) and not adhesive failure between the tissue and gel. Frequency-dependent rheological characterization and tissue adherence data for Pluronic F-127, a commercial thermoreversible synthetic hydrogel that has been clinically applied for PAs (*24*, *43*), and ECM hydrogel show that Pluronic F-127 is stiffer when compared with ECM hydrogel on the basis of peak storage modulus (G' 9159 ± 970 Pa versus 391 ± 120 Pa; $P < 0.0001$) but has yield behavior similar to that of ECM hydrogel (157 Pa) (fig. S5). Proteomic analysis of the ECM hydrogel showed that among the proteins detected, collagen 1 (represented by COL1A1 and COL1A2) has a relative abundance multiple orders of magnitude higher than other proteins, indicating a collagen-enriched ECM hydrogel sample (Fig. 2E).

ECM hydrogel attenuates MMT caused by exposure to cyclic mechanical stretch

To explore the potential role of the ECM hydrogel to interfere with MMT induced by mechanical stimuli, we used an in vitro experimental model where HPMCs were exposed to cyclic stretching conditions and then expression patterns of recognized MMT-related markers were analyzed. HPMCs were plated on uncoated or ECM hydrogel–coated plates (Fig. 3A). HPMCs on control substrates and subjected to mechanical stretch acquired an elongated morphology and a down-regulation in the expression of the tight junction protein ZO-1 as compared with HPMCs under static conditions. In contrast, HPMCs exposed to mechanical stretch on ECM hydrogel–coated plates retained a morphology similar to that of the static controls and maintained ZO-1 expression. The mesenchymal conversion of HPMCs induced by mechanical stretch was further supported by a significant down-regulation of E-cadherin (*CDH1*) ($P < 0.001$) and up-regulation of *SNAI1* ($P < 0.001$), matrix components such as *COL1A2* ($P < 0.05$) and *FN1* ($P < 0.001$), *MMP2* ($P < 0.05$), *TGFB1* ($P < 0.01$), and vascular endothelial growth factor A (*VEGFA*) ($P < 0.001$) as compared with gene expression under static conditions (Fig. 3B). The ECM hydrogel coating prevented the mechanical induction of MMT-related genes in HPMCs exposed to stretch. Moreover, no significant changes ($P > 0.05$) in gene expression were observed in HPMCs adhered to the ECM hydrogel coating in the absence of mechanical stimulus (static conditions) as compared to cells cultured on an uncoated surface under static conditions (Fig. 3B). The variability observed between replicates in the reverse transcription–quantitative polymerase chain reaction (RT-qPCR) studies could be a consequence of interindividual differences between HPMC donors ($n = 3$).

To rule out any specific effect of applying the ECM hydrogel to the basal side of the cells, ECM was applied as a hydrogel onto the apical side of a mesothelial monolayer of human MeT5A cells. ECM hydrogel overlay also suppressed MMT caused by mechanical stretch in a concentration-dependent manner (fig. S6). Taking together these results suggests that the ECM hydrogel can interface with cells through both the basal and apical sides of MCs to protect them from the MMT conversion induced upon exposure to mechanical stretch.

ECM hydrogel retention at the site of application and tissue adherence

The retention time for ECM hydrogel on peritoneal tissue was tracked with a fluorescent label. In a first study, mice were treated postoperatively with maleimide 680–labeled ECM hydrogel and imaged on days 1, 2, 3, 4, and 6 by in vivo imaging system (IVIS). After application, ECM hydrogel displayed intense fluorescent signal in the peritoneum. The signal was constant over the course of the study, suggesting that the ECM hydrogel was not absorbed and persisted in the local peritoneal area through the duration of the study (Fig. 4A). Further, on day 6, the ECM hydrogel coverage remained localized to the site of injury as evidenced by fluorescent imaging and histology of parietal peritoneal excised tissues (Fig. 4, B and C). Histological evaluation of the parietal peritoneal tissue 15 days after surgery showed that the ECM hydrogel is retained at the site of application and remains adhered to the parietal peritoneal tissue for long time frames (fig. S7). Because the reported pathophysiology for PA formation occurs within 5 to 10 days after surgery (acute stimulus) (*44*), the ECM hydrogel retention time frame is compatible for coverage and adhesion prevention in the peritoneal cavity.

ECM hydrogel reduces PAs and interferes with MMT in a preclinical mouse model

We examined whether application of the ECM hydrogel to peritoneal ligations could interfere with the development of PAs in an IB-based mouse model (*14*) compared with Pluronic F-127 hydrogel. Both hydrogels were easily sprayed onto the IBs, enabling uniform coverage of the tissue, and hydrogel application was completed in less than 30 s. After 5 days, the attachment of adhesions to the IBs was scored. There were severe adhesions in the untreated control group, demonstrating the ability of the IB model to generate robust

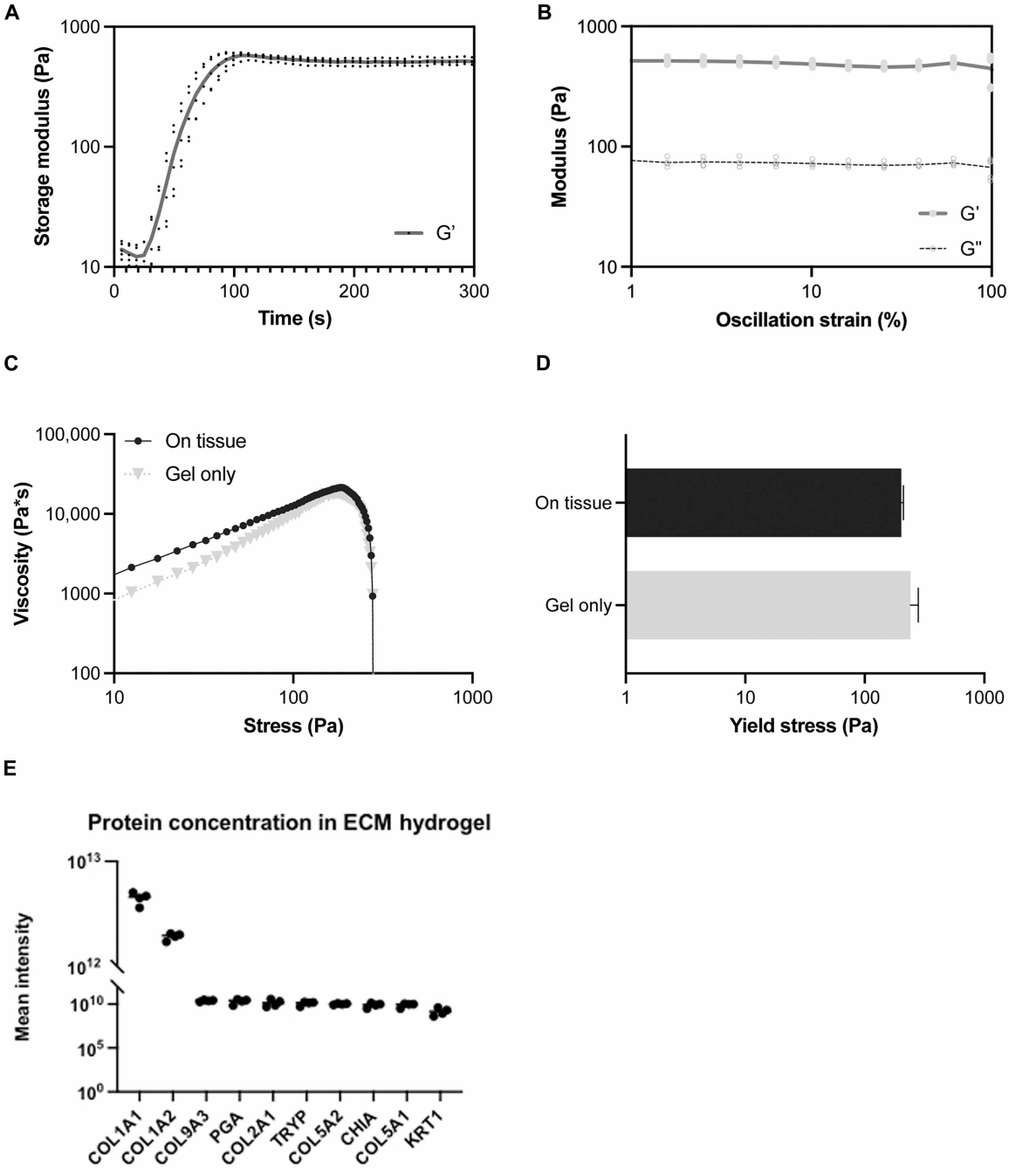

Fig. 2. ECM hydrogel demonstrates rapid gelation, mechanical stability under strain, tissue adhesion, and preservation of matrix proteins. (**A**) Gelation kinetics of ECM hydrogel storage modulus (G′) at 37°C showed complete gelation within 2 min ($n = 5$). Data are presented as mean line and independent samples as dots. (**B**) Strain-dependent ($\omega = 10$ rad/s, 37°C) shear rheology of ECM hydrogel ($n = 5$). Data are presented as mean lines of storage modulus (G′) and loss modulus (G″). Dots represent replicates. (**C**) Representative yield stress behavior of ECM hydrogel was measured in a standard parallel-plate geometry and on tissue (pig intestine) in a stress-ramp experiment performed at a rate of ~1.5 Pa/s to determine adhesion of ECM hydrogel to tissue. Data shown are from a single representative tissue sample. (**D**) Yield stress average values of ECM hydrogel formulations obtained from the peak viscosity observed in the stress ramp. Data are presented as mean ± SEM, $n = 10$ per condition. (**E**) Graphical representation of the mean protein concentrations for the top 10 proteins, ranked by their mean intensity values. Each data point represents one protein, with the plotted value corresponding to the mean intensity measured across four independent batches. The intensity values are used as a proxy for protein concentrations. Data are presented as mean ± SD.

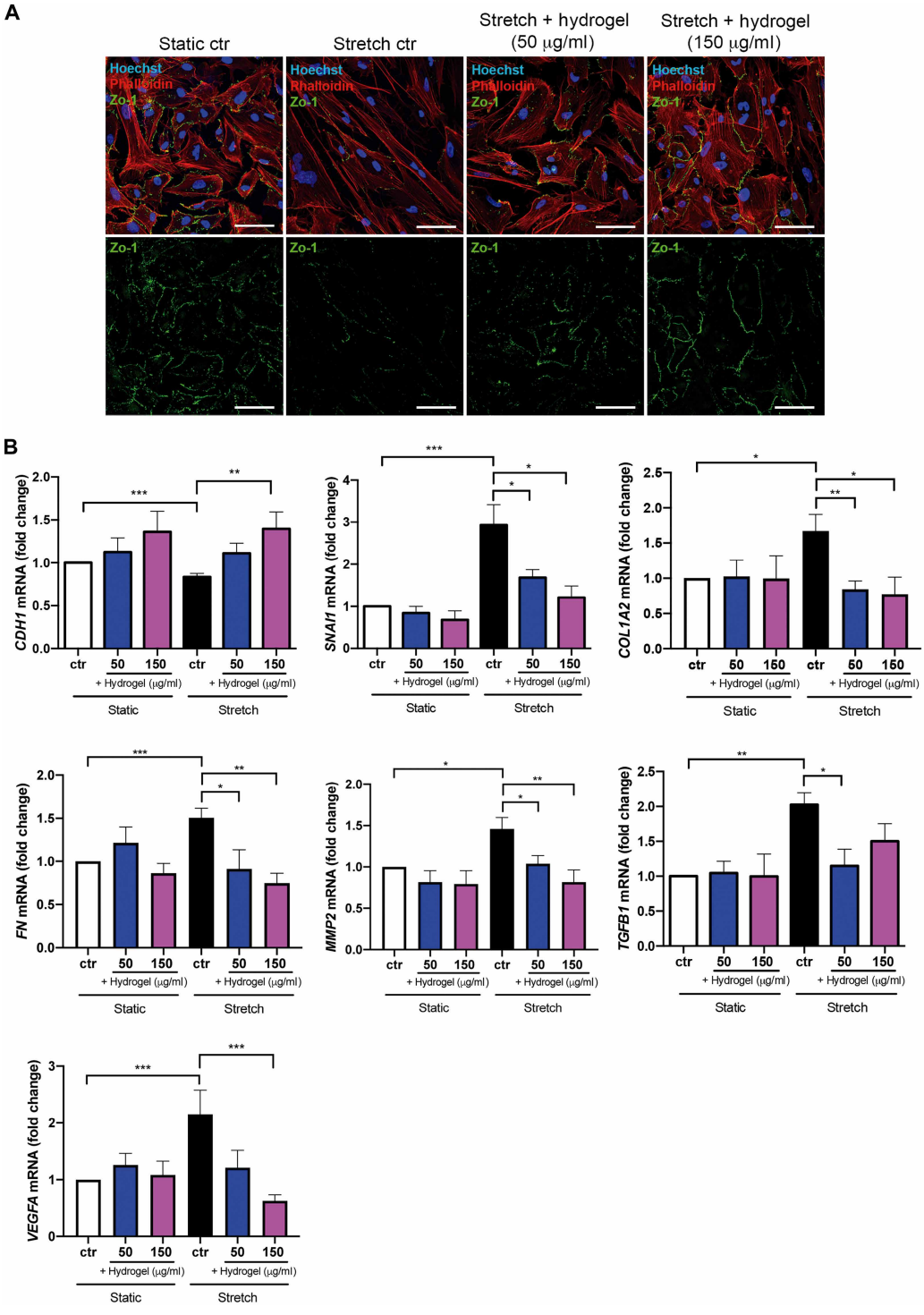

Fig. 3. ECM hydrogel coating reduces mechanical stretching–induced MMT in vitro. HPMCs were cultivated on uncoated (ctr) or ECM hydrogel-coated (+ hydrogel) flexible plates and exposed to static or stretch conditions for 48 hours posttreatment to induce MMT. (**A**) Representative immunofluorescence images of phalloidin (red) and ZO-1 (green) in cells plated on flexible plates (50 and 150 μg/ml). Scale bars, 50 μm. (**B**) RT-qPCR analyses of *CDH1*, *SNAI1*, *COL1A2*, *FN*, *MMP2*, *TGFB1*, and *VEGFA* show that the ECM hydrogel blocks the MMT induced by mechanical stretch stimulus in a concentration-dependent manner (50 and 150 μg/ml). Bars represent the mean ± SEM of duplicate determinations in three independent experiments and three different HPMC donors. Analysis by Kruskal-Wallis test with post hoc Mann-Whitney rank-sum *U* test. $*P < 0.05$, $**P < 0.01$, and $***P < 0.001$.

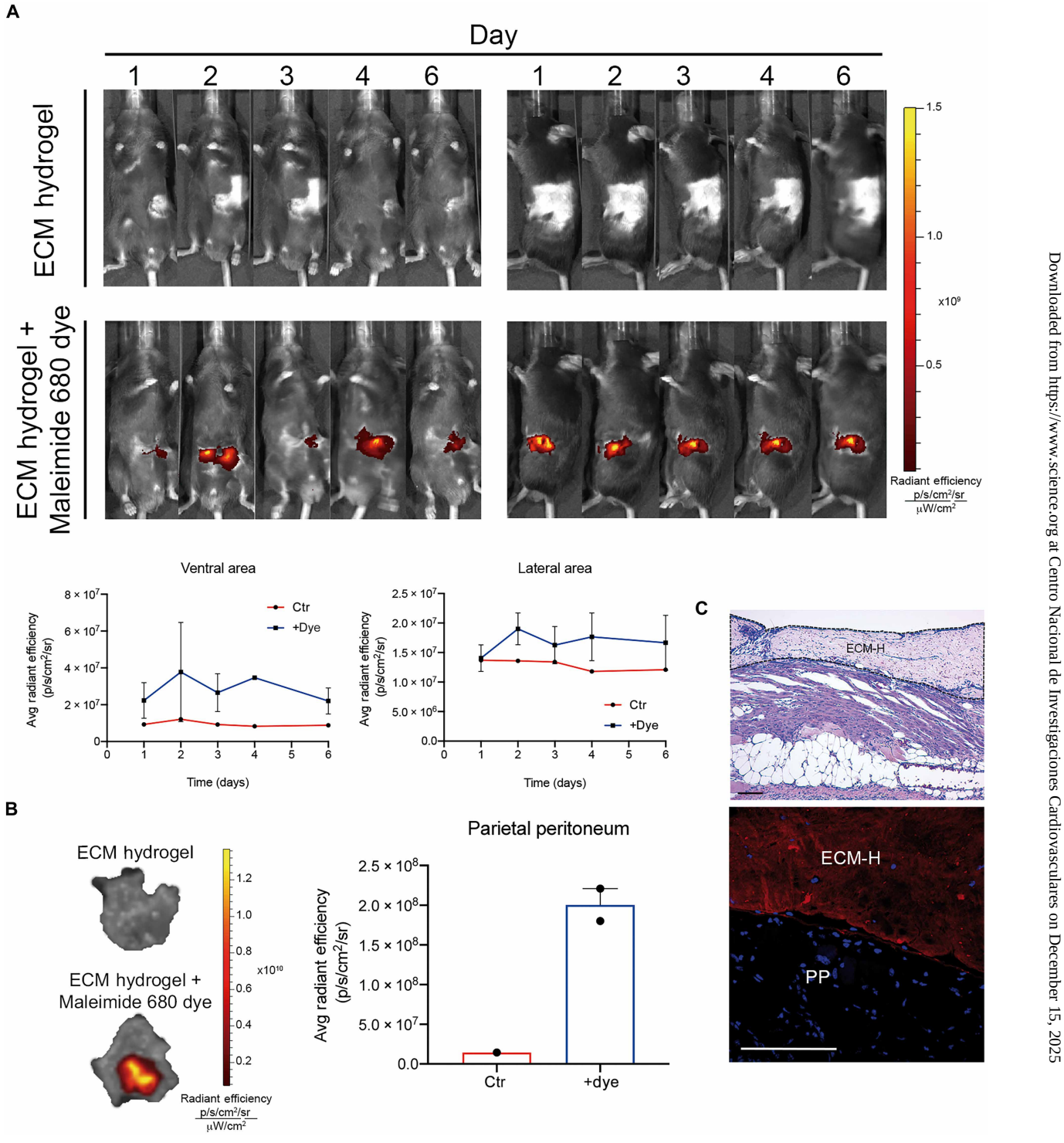

Fig. 4. ECM hydrogel retention at the site of application. (**A**) Representative images show fluorescence signal in ventral (left) and lateral peritoneal areas (right) of a mouse inoculated with the ECM hydrogel alone or with ECM hydrogel labeled with fluorescent dye Maleimide 680. Summary of radiant efficiency of the labeled ECM hydrogel in ventral and lateral view over the time (expressed as photons per second per square centimeter per steradian). Error bars represent the SEM of two mice in the "+ dye" group, $n = 1$, control. (**B**) Imaging of ex vivo parietal peritoneal tissues after euthanasia shows fluorescent signal covering the IB (left). Bar graph represents the average radiant efficiency detected (right). Ctr: control mouse inoculated with ECM hydrogel alone; + dye: mice inoculated with ECM hydrogel labeled with fluorescent dye. Error bars represent the SEM of two mice in the "+ dye" group, $n = 1$, control. (**C**) Hematoxylin and eosin staining shows that the ECM hydrogel (outlined area) adhered to the surface of the peritoneum. Bottom: Fluorescence image shows that the ECM hydrogel labeled with Maleimide 680 dye (red) adhered to the parietal peritoneal surface. Nuclei are marked with 4′,6-diamidino-2-phenylindole (DAPI; blue). Scale bars, 100 μm. ECM-H, ECM hydrogel; PP, parietal peritoneum.

adhesions. The grade, tenacity, and overall score of the IB adhesions (table S1) (*14*) were significantly ($P < 0.01$) diminished in both hydrogel-treated groups as compared with the control group (Fig. 5, A and B). In histological sections of the IB zones after 5 days, the ECM hydrogel was found to cover the IB in all samples. ECM hydrogel thickness in histological sections had an average value of 461.2 μm ± 41.8 (mean ± SEM). The Pluronic F-127 hydrogel was not detected in histological sections, likely because of degradation during tissue sample processing, given that it is a synthetic hydrogel (Fig. 5C). Adhesions assessed 15 days after surgery were more mature than at the 5-day time point; however, the ECM hydrogel maintained significant protection for grade ($P < 0.001$) and overall score ($P < 0.01$) of PAs (table S1) (*14*) compared with the control group (fig. S8).

To verify whether ECM hydrogel treatment interferes with MMT and preserves peritoneal membrane structure, we analyzed mesothelial (CK) and myofibroblast (α-SMA) markers by immunohistochemistry 5 days after surgery. Our findings revealed that the mesothelial monolayer (CK^+) was mainly preserved in mice receiving ECM hydrogel as compared with control or Pluronic F-127 groups. In all peritoneal samples from mice treated with ECM hydrogel, we observed a mesothelization on the ECM hydrogel covering the IB zones (Fig. 6A). With the ECM hydrogel, we observed that CK^+ cells restricted to an organized mesothelial layer, whereas in the Pluronic F-127 hydrogel group, the CK^+ cells appeared at the mesothelial border and in the submesothelial space and were more disordered than the ECM hydrogel. PA tissues from control mice showed a significant increase in positive submesothelial areas for CK ($P < 0.05$) and α-SMA ($P < 0.01$) as compared with tissues from mice receiving ECM hydrogel treatment (Fig. 6A and fig. S7). Although the Pluronic F-127 group showed significant staining for CK ($P < 0.01$) in the submesothelial zones as compared with the ECM hydrogel group, the coexpression of α-SMA in those same areas was lower than in control mice (Fig. 6A).

These results were supported by dual-immunofluorescence analysis of peritoneal tissues, with CK and fibroblast marker fibroblast–specific protein-1 (FSP-1, also called S100A4). CK staining was confined to a mainly preserved MC monolayer in mice treated with ECM hydrogel, whereas an increased submesothelial costaining of CK and FSP-1 was observed in control and Pluronic F-127 mice (Fig. 6B). These data support a protective role for the ECM hydrogel in preventing loss of the MC layer and reducing the accumulation of submesothelial $CK^+/FSP\text{-}1^+$ cells.

ECM hydrogel coating alters local tissue inflammatory response in the PA mouse model

Formation of a proregenerative immune microenvironment supports the development of proper replacement tissue; however, unbalanced activation of the immune response can produce fibrosis or damaging inflammation, which may cause excessive tissue tethering (*45*). To evaluate the inflammatory response to the ECM hydrogel, a panel of inflammation-related genes in IB tissue samples was evaluated (fig. S9). We found a significant ($P < 0.001$) decrease in the expression of the proinflammatory cytokine *Il1b* in ECM hydrogel treated 5 days after surgery in mice as compared with the control group (Fig. 7A). Similarly, we found a significant enrichment in several inflammation-associated canonical signaling pathways in both HPAMCs and MPAMCs in our RNA-seq datasets ($P < 0.05$) (Fig. 7B). *IL1B* up-regulation was present in these inflammation-associated pathways, highlighting its important role in MMT and PA formation (data file S1). The expression of other important mediators of the inflammatory response, including *Tgfb1*, *Tnf*, *Mcp1*, *Il17a*, *Il33*, *Nfkb1*, and *Il6*, was also evaluated (fig. S9); however, no differences were detected in the ECM hydrogel group as compared to control mice. The sutures used to form IBs could mask, at least in part, the anti-inflammatory effect of the ECM hydrogel. A significant up-regulation of *Tgfb1*, *Mcp1*, and *Il33* inflammatory-related genes was observed in mice receiving Pluronic F-127 as compared with the control and ECM hydrogel groups. This effect could be attributed to the synthetic nature of Pluronic F-127.

Peritoneal tissues were also evaluated for $CD45^+$ cells (a pan–immune cell marker) by immunohistochemical staining. The recruitment of $CD45^+$ cells into the damaged tissue was significantly lower in the ECM hydrogel experimental group than in control ($P < 0.001$) and Pluronic F-127 mice ($P < 0.05$) (Fig. 7C), demonstrating a reduced overall inflammatory response. In summary, these data support the hypothesis that application of the ECM hydrogel aids in creating a balanced healing microenvironment through the mediation of inflammatory and immune responses.

ECM hydrogel supports a reduction in PAs and MMT in a uterine horn abrasion rabbit model

The capacity of ECM hydrogel to support a reduction in adhesion formation was also evaluated in a uterine horn abrasion rabbit model. This experimental model is frequently referenced in the literature as an appropriate choice for evaluating materials for prevention of postsurgical adhesions after abdominal surgery (*46*). Our results showed that the application of ECM hydrogel leads to a reduction in PAs in terms of area and strength as compared with the control group (Fig. 8, A and B). Moreover, signs of MMT, including submesothelial costaining of CK and α-SMA, were more frequently observed in the control group as compared with the ECM hydrogel–treated animals (Fig. 8C). The lack of ECM hydrogel material in histological samples could be attributed to the removal of at least part of the serosa layer during the abrasion of the uterine horns. On the basis of the study performed in mice, we evaluated CD45 in transverse sections of rabbit uterus. Our results show a significant ($P < 0.05$) inflammation-associated staining in the control group as compared with animals receiving the ECM hydrogel (fig. S10). These results corroborate the findings described above in an alternative in vivo model of PA formation and further support that the ECM hydrogel reduces inflammatory and fibroblastic features of injured peritoneal tissues.

DISCUSSION

Although some of the molecular processes involved in PA development are still unknown, recent investigations have shown that adhesions can originate from MCs through a MMT process (*14*, *20*). Here, we analyzed the myofibroblastic conversion of MCs in patient-derived postsurgical adhesions and that induced in a standardized PA mouse model. Specifically, our study revealed the acquisition of an elongated fibroblast-like phenotype in HPAMCs and MPAMCs. Pattern analysis of the whole transcriptome in HPAMCs revealed enrichment in several canonical signaling pathways related to postsurgical PA formation, including the regulation of the MMT pathway. An enrichment of specific EMT/MMT canonical pathways, including gap junction signaling and epithelial adherens junction signaling, supports the myofibroblast conversion of MCs. These

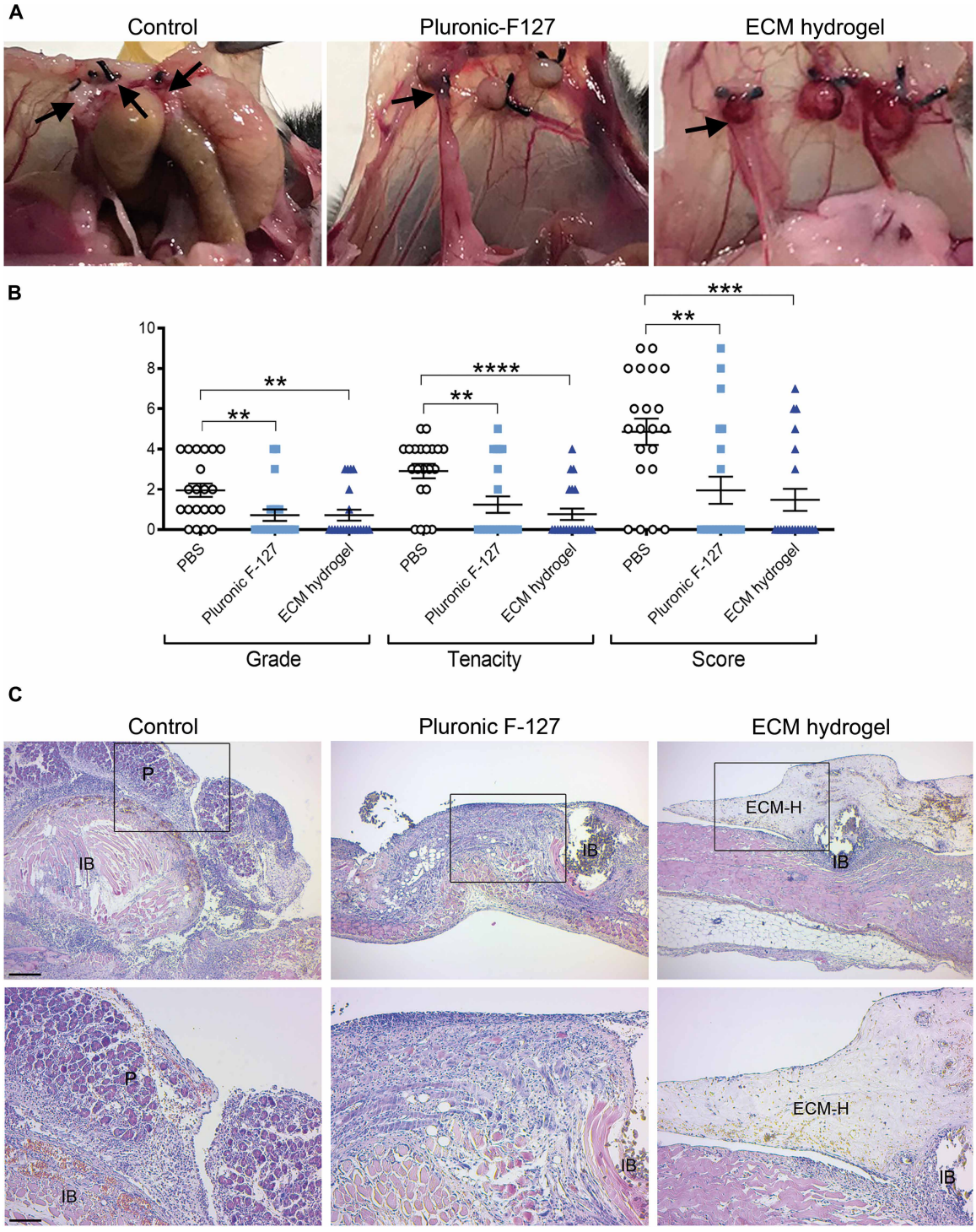

Fig. 5. ECM hydrogel treatment ameliorates PA formation in mice. (**A**) Representative pictures of PAs 5 days after injury. In the control group, black arrows show three PAs formed between parietal and visceral serosa layers. Left arrow, PA to peritoneal fat (grade, 4; tenacity, 4; score, 8); middle and right arrows, PAs to colon (grade, 4; tenacity, 5; score, 9). In the Pluronic F-127 group, arrow shows one PA to the peritoneal fat (grade, 3; tenacity, 4; score, 7). In the ECM hydrogel group, arrow shows one thin adhesion to the peritoneal fat (grade, 1; tenacity, 2; score, 3). Arrows point to the zone of adhesion of visceral tissues to IBs. (**B**) Quantification of adhesions by grade, tenacity, and overall score following a point scale (table S1) (*14*). Graph shows individual values for each IB (three IBs per mouse and eight mice per group). Bars represent the mean ± SEM. Analysis by Kruskal-Wallis test with post hoc Mann-Whitney rank-sum *U* test. $^{**}P < 0.01$, $^{***}P < 0.001$, and $^{****}P < 0.0001$. (**C**) Histological analysis of mouse peritoneal samples. Hematoxylin and eosin staining shows a PA zone to the pancreatic tissue in a control mouse (left). A submesothelial fibrotic zone adjacent to an IB can be observed in a mouse receiving Pluronic F-127 (middle). An ECM-based scaffold is completely covering the IB in a mouse receiving ECM hydrogel (right). PBS, phosphate-buffered saline; P, pancreas. Scale bar, 250 μm. Bottom row of images represents higher magnification (scale bar, 100 μm) of the corresponding delimited areas in the top row.

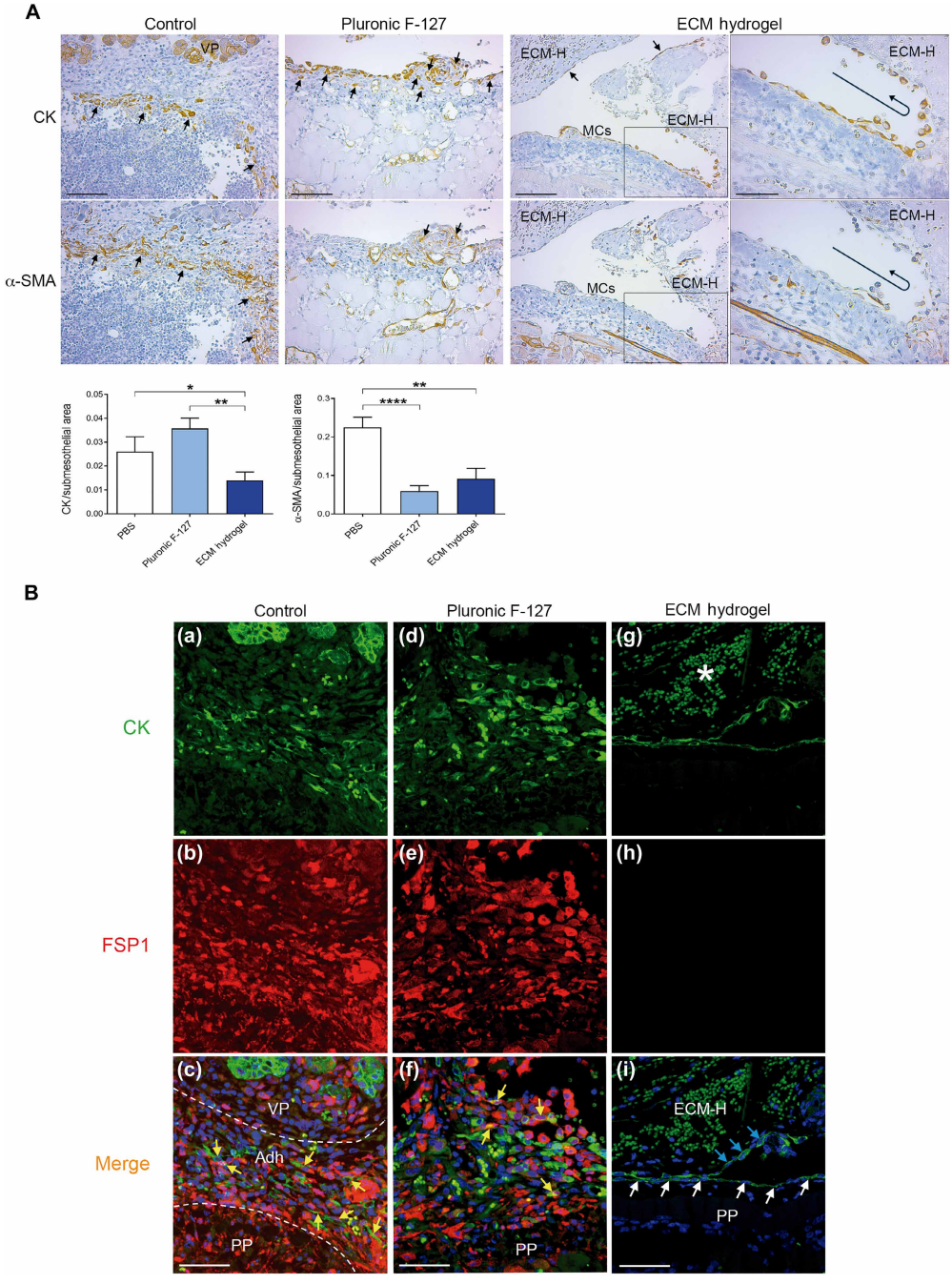

Fig. 6. ECM hydrogel interferes with MMT and preserves peritoneal membrane structure in mice. (**A**) Immunohistochemical analysis of mouse parietal peritoneal tissues adjacent to IB areas in each group. Staining of serial sections was performed for CK and α-SMA. Left column: Arrows point to a PA area with strong expression of CK and α-SMA in serial sections of a control mouse. VP, visceral peritoneum. Scale bars, 100 μm. The peritoneal surface is completely covered by the adhesion (fig. S7). Middle column: Arrows point to MCs expressing CK in the submesothelial zone of a mouse treated with Pluronic F-127 (top). Arrows point to few areas of submesothelial α-SMA staining overlapping with CK^+ zones (bottom). Capillaries of a highly vascularized submesothelial zone are stained for α-SMA. Scale bars, 100 μm. Right two columns: Pictures show a peritoneal sample from a mouse treated with the ECM hydrogel, where a CK^+ mesothelium is preserved. The ECM hydrogel was mainly mesothelialized by cells, which are CK^+ (arrows). The curved arrow indicates the direction of mesothelialization of the ECM hydrogel from the peritoneal mesothelial monolayer. The staining for α-SMA was restricted to a few submesothelial resident myofibroblasts, small capillaries, or deep muscle bundles. Scale bars, 100 μm (left) and 50 μm (right). Bottom: Submesothelial CK and α-SMA staining quantification. Bars represent the mean ± SEM. Analysis by Kruskal-Wallis test with post hoc Mann-Whitney rank-sum *U* test. $*P < 0.05$, $**P < 0.01$, and $****P < 0.0001$; $n = 2$ IBs per mouse; $n = 8$ mice per group. (**B**) Representative double-immunofluorescence images of parietal peritoneal tissues adjacent to IB areas for each mouse group. Immunostaining was performed for CK (green) and FSP-1 (red), and nuclei are marked with DAPI (blue). Yellow arrows, double $CK^+/FSP\text{-}1^+$ cells. White broken lines delimit the adhesion area (Adh). Asterisk shows autofluorescent erythrocytes accumulated in the ECM-hydrogel compartment. Light blue arrows, MC monolayer ($CK^+/FSP\text{-}1^-$) lining the ECM hydrogel. White arrows, MC monolayer ($CK^+/FSP\text{-}1^-$) lining the parietal peritoneum. The corresponding Maleimide-680 overlay is shown in Fig. 4C to confirm spatial coincidence.

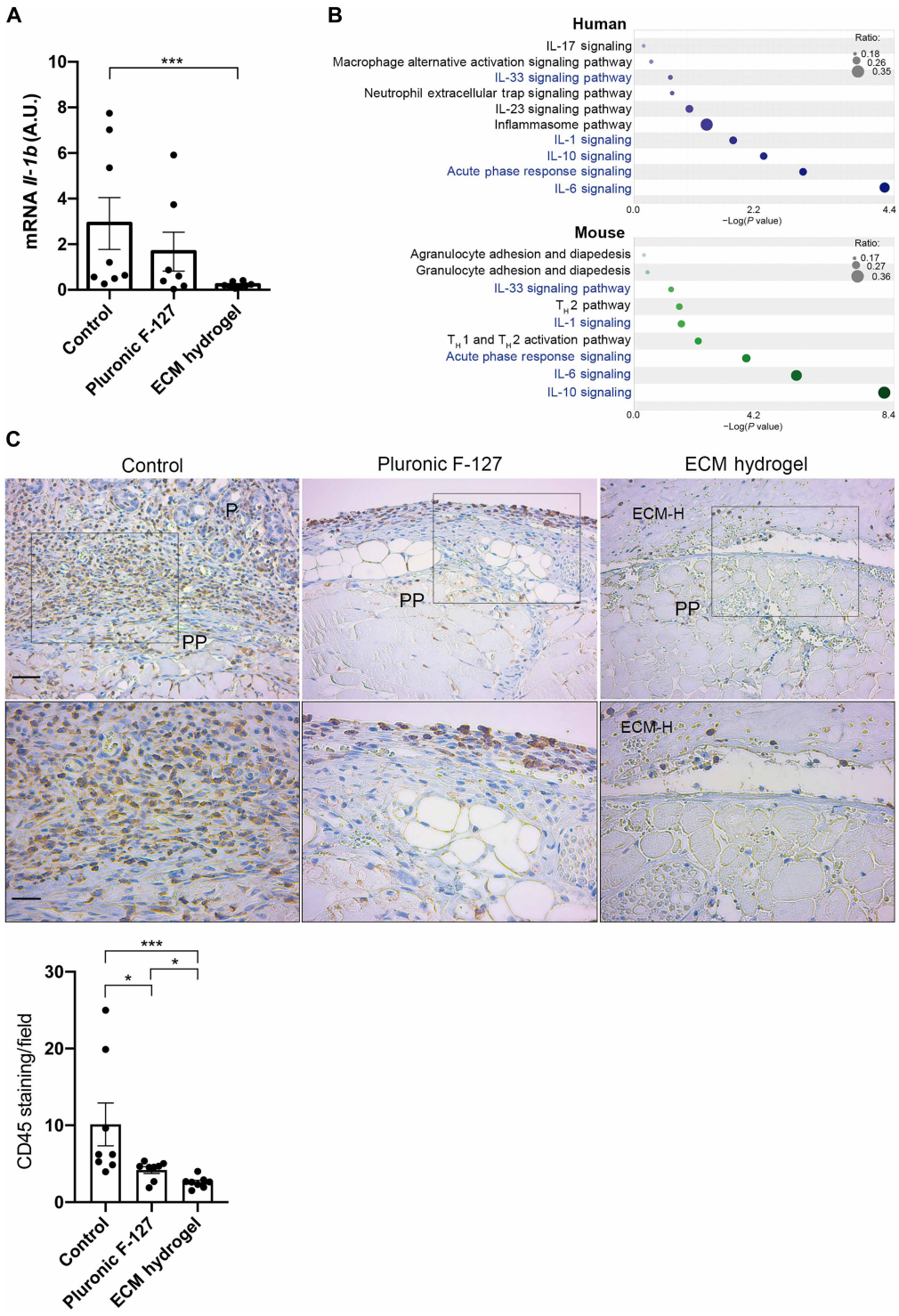

Fig. 7. Anti-inflammatory properties of the ECM hydrogel. (**A**) RT-qPCR analysis of *Il1b* in mouse IB tissue samples. Data are presented as mean ± SEM; control, $n = 8$; Pluronic F-127, $n = 7$; ECM hydrogel, $n = 8$; analysis by Kruskal-Wallis test with post hoc Mann-Whitney rank-sum *U* test. ***$P < 0.001$; A.U., arbitrary units; IL-1β, interleukin-1β. (**B**) RNA-seq bubble charts showing significantly differentially regulated canonical pathways associated with inflammation and analyzed with IPA software in HPAMCs (top) and MPAMCs (bottom) as compared with HPMCs and MPMCs, respectively. Shared canonical pathways for patients and mice are presented in blue. The *x* axis indicates the statistical significance, calculated using the Benjamini-Hochberg correction. Color intensity of bubbles represents –log (*P* value). Size of bubbles represents the ratio of overlapping genes to total genes in the pathway. T_H1, T helper cell 1. T_H2, T helper cell 2. (**C**) Representative images of CD45 staining in mouse parietal peritoneal zones adjacent to IBs from the control, Pluronic F-127, and ECM hydrogel groups. Scale bar, 100 μm. The insets represent a higher magnification of the corresponding delimited area (bottom). Scale bar, 50 μm. Few $CD45^+$ inflammatory cells were found in the ECM hydrogel group. They were mainly retained in the ECM hydrogel compartment. Bottom: Graphic showing CD45 staining quantification. Bar shows mean ± SEM; $n = 8$ per group; analysis by Kruskal-Wallis test with post hoc Mann-Whitney rank-sum *U* test. *$P < 0.05$ and ***$P < 0.001$.

MMT-related signaling pathways were comparable to those observed in MPAMCs. Our results demonstrate a repression of typical mesothelial genes and up-regulation of fibroblast-associated genes in cells isolated from both human and mouse fibrotic adhesions. Both RNA-seq studies revealed a robust TGF-β1 signaling activation, with induction of its effectors *GREM1*, *TGFB1*, *TGFBR1*, *SNAI1*, and *MMP2*. Chronic peritoneal diseases, such as fibrosis associated with peritoneal dialysis or peritoneal metastasis, have been traditionally linked to induction by biochemical pathways, mainly TGF-β1 (*47*, *48*). Meanwhile, mechanical forces have been recognized as important drivers of the MMT process in acute peritoneal injuries caused during abdominal surgery procedures (*21*). Specifically, we recently reported that CAV1 and yes-associated protein (YAP) drive mechanically induced MMT-associated peritoneal fibrosis (*21*). Here, mechanically

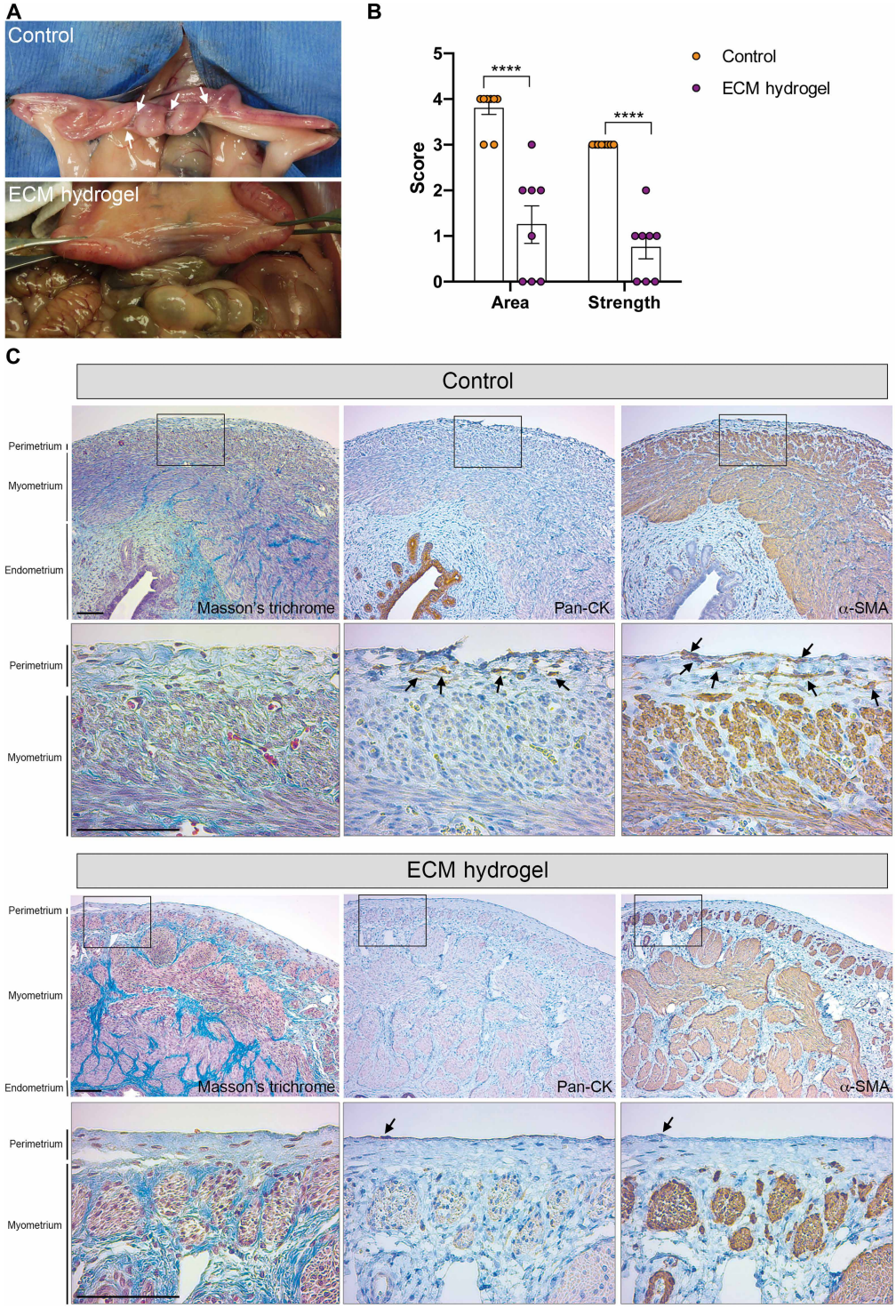

Fig. 8. ECM hydrogel ameliorates MMT and adhesions in a uterine horn abrasion rabbit model. (**A**) A representative picture from the control group (top) shows multiple adhesions binding the serous layer of the uterine horn zone at different points (arrows). No relevant adhesions were observed in the ECM hydrogel experimental group (bottom). (**B**) Score of adhesions in terms of area and strength. Left and right uterine horns were evaluated for each animal (control group: five animals; ECM hydrogel group: four animals). Analysis by Mann-Whitney rank-sum *U* test. ****$P < 0.0001$. (**C**) Representative images of transversal uterine serial sections from the control group: Masson's trichrome (left), CK (middle), and α-SMA (right). Scale bar, 100 μm. Deep endometrium epithelium was stained for CK and myometrium was stained for α-SMA. The insets (bottom) represent a higher magnification of the corresponding delimited areas. Scale bar, 50 μm. Arrows point to MMT submesothelial areas as revealed by the overlap in staining for CK and α-SMA. Representative images of transversal uterine serial sections from the ECM hydrogel group: Masson's trichrome (left), CK (middle), and α-SMA (right). Scale bar, 100 μm. The insets (bottom) represent a higher magnification of the corresponding delimited areas. Scale bar, 50 μm. Arrows point to a $CK^+/\alpha\text{-SMA}^-$ MC zone in monolayer position.

induced MMT overlapped with *YAP/TAZ* target gene subset (Hippo signaling pathway). In addition, exposure of CAV1-deficient MCs to cyclic stretch leads to a robust up-regulation of MMT-related gene programs, which is blunted upon TGF-β1 inhibition (*21*, *22*). In accordance with these data, we found dysregulations in both caveolar and Hippo signaling pathway–associated mechanical gene subsets. YAP/TAZ can cooperate with TGF-β1 to promote expression of genes involved in MMT induction such as *SERPINE1* (also known as *PAI-1*), *ankyrin repeat domain 1* (*ANKRD1*), *SNAI1*, *MMP2*, *CD44*, *FAT atypical cadherin 4* (*FAT4*), and *WW domain containing transcription regulator 1* (*WWTR1*). In addition, YAP/TAZ can induce the expression of CAV1, which limits excessive MMT; and prolonged exposure to TGF-β1 can down-regulate CAV1. In this regard, our RNA-seq studies also show relevant dysregulations in target genes shared by the

caveolar and TGF-β1 pathways, such as *ACTA2*, *CAV1*, and integrin-encoding genes. These results suggest that the conversion of MCs to myofibroblasts, which takes place during the formation of PAs, is the result of cooperation between biochemical and biomechanical signals as a consequence of the mechanically induced injury during intra-abdominal surgeries.

Moreover, the IB-based mouse model has been previously referenced as a hypoxia standard (*20*, *49*). Here, we noted up-regulation of *HIF1A* (*hypoxia-inducible factor-1*α) in HPAMCs and MPAMCs. Presumably, up-regulation of the proangiogenic factor VEGFA could trigger a hypoxia-associated vascularization response as observed in patients (*14*). Together, these data suggest that the IB-based mouse model for the generation of PAs is a faithful reflection of the MMT-related changes that occur in patients with PAs, despite the different profiles in terms of gene expression, adhesion, migration, and invasion that might exist between the visceral and parietal MCs in physiological conditions (*50*, *51*).

The lack of studies comparing the gene expression profiles of MMT-derived fibroblasts and non–MMT-derived fibroblasts limits in part the precise knowledge of the contribution of the MMT process to the formation of PAs. In this regard, genetic lineage tracing of WT1-expressing MCs after surgical injury in mice confirmed that MCs adopt a mesenchymal phenotype and migrate into the subserosa (*52*). Alternative lineage tracing approaches and intravital imaging show that the $PDPN^+$ mesothelium contributes to and is incorporated into PAs (*20*, *31*). In addition, immunohistochemical studies of clinical PA biopsies can give us a rough idea of the contribution of MMT-derived fibroblasts to PAs. Our findings support that the conversion of $PDPN^+$ MCs into $PDPN^+$ myofibroblasts is a relevant event, despite the fact that other minority populations—including endothelial-to-mesenchymal transition–derived fibroblasts, fibrocytes recruited from the bone marrow, or resident fibroblasts—could also contribute to PAs (*48*).

The PA mouse strategy evaluated here represents an adequate model not only to delve into the molecular and pathological mechanisms that govern postsurgical adhesions but also to develop preclinical studies of possible therapeutic strategies. Currently, no treatments have been proven to prevent or reduce the formation of postsurgical PAs. Although a variety of materials, such as Seprafilm (sodium hyaluronate/carboxymethylcellulose sheet) or Interceed (oxidized regenerated cellulose), have demonstrated limited success for preventing the severity of adhesions (*53*), a new generation of hydrogel barriers with proven tissue adherence and antiadhesion efficacy is emerging (*33*). We developed a new ECM hydrogel with liquid gel barrier characteristics. In general terms, other tissue protector materials lack longevity at the surgically injured site, and physical barriers, such as films or sheets, are difficult to handle and apply. Here, we first evaluated the effect of ECM hydrogel on the MMT process induced by mechanical stretch stimuli in vitro (*21*). HPMC culture plates coated with ECM hydrogel were able to substantially block the transition to a fibroblast-associated phenotype, as well as the induction of classical mesenchymal genes, suggesting that total or partial blockade of MMT induced by mechanical damage could be a new therapeutic option to effectively prevent postsurgical PA formation (*14*, *54*). Furthermore, the ECM hydrogel did not change basal MMT-related gene expression under static conditions, which means that it is harmless to cells under physiological conditions. This observation could be due to the fact that the ECM hydrogel was obtained from solubilization of ECM from bone tissues. This natural origin of materials could present advantages compared with alternative synthetic adhesion barriers, which can interfere with adhesion formation but have also been shown to increase the risk of infection (*55*). In addition, the ECM hydrogel was applied onto the monolayer of MCs in mechanical stretching experiments in vitro at concentrations similar to those used in vivo. Our findings suggest that the ECM hydrogel can modulate MMT-related signaling pathways in a similar manner whether it is present on the apical or basal side of MCs.

The main drawback of physical barriers is that they frequently move from the administration site (*55*). Our study showed that after application of the ECM hydrogel in the postsurgical PA mouse model, a film covering the IB ligation zone remains for at least 15 days. These data suggest that the ECM hydrogel could enable successful mesothelial wound healing, because this process is estimated to be resolved within ~5 to 10 days after peritoneal injury (*6*, *55*).

The administration of the ECM hydrogel on peritoneal induced lesions in mice supported more than 75% reduction in the severity of PAs compared to the untreated group. This prophylactic action is due at least in part to a barrier effect that avoids direct contact between parietal and visceral peritoneal tissues. However, histological studies revealed the cellular impact of the ECM hydrogel microenvironment, which was characterized by an intact mesothelial monolayer with the low presence of MC-derived myofibroblasts in the submesothelial layer as compared to the control group. These findings were also favorably compared to mice receiving Pluronic F-127, a synthetic and thermoreversible hydrogel that has been previously shown to ameliorate PAs by acting as a tissue barrier (*24*, *43*). The presence of submesothelial CK^+ cells costained with FSP-1 suggests that, although Pluronic F-127 reduced PA formation, it did not modulate the MMT process. FSP-1 has been reported to be mainly confined to transitioning fibroblasts, whereas α-SMA predominates in, but is not limited to, morphologically and functionally mature myofibroblasts, which could explain why submesothelial CK^+ fibroblasts expressing α-SMA were less abundant than $FSP\text{-}1^+$ cells in the Pluronic F-127 group (*17*, *56*–*58*). Our results suggest that both hydrogels (ECM hydrogel and Pluronic F-127) show an adhesion barrier effect, whereas only ECM hydrogel creates a microenvironment that alters MMT-related processes and that both the barrier and the MMT-modulating functions may be relevant for the prophylactic effect of the ECM hydrogel. These findings are reinforced by a depletion study targeting MCs, performed in a similar IB-based mouse model, where PA development was reduced (*20*). Taking these data together suggests that the MMT of peritoneal MCs constitutes an important mechanism during the development of PAs.

The ECM is a complex acellular environment present in all tissues and is crucial for their repair; it acts as a support that favors wound healing and regeneration and provides a space for cell signaling (*59*). Exposure of an ECM fragment (laminin β1-chain) to the mesothelium abrogated the release of active MMP2 and rescued peritoneal membrane integrity in peritoneal fibrosis (*60*). Here, we found that the ECM hydrogel constitutes a natural scaffold that permits mesothelization as demonstrated by the formation of a mesothelial monolayer (CK^+/α-SMA^-/$FSP\text{-}1^-$). The properties of this de novo mesothelium could prevent, at least in part, adhesions between damaged peritoneal tissues.

We also investigated the ECM hydrogel scaffold immune microenvironment (*61*). Our data indicate that the application of ECM hydrogel results in decreased expression of *Il1b* in the injured peritoneal tissue compared with controls. In particular, we found that inflammation was notably less in tissues coated with ECM

hydrogel, as was the expression of *Il1b* when compared with synthetic hydrogel material Pluronic F-127. Interleukin-1β has been described as an inducer of the MMT process that acts by reinforcing TGF-β1 signaling (*16*, *17*, *57*, *62*). These data are aligned with immunohistochemical analysis of peritoneal tissues for CD45, a pan–immune cell marker, 5 days postoperation, which revealed fewer $CD45^+$ cells in the ECM hydrogel group compared with both control and Pluronic F-127–treated mice, suggesting effective healing with ECM hydrogel and inflammation with synthetic hydrogel. In addition, our data revealed that Pluronic F-127 has a markedly increased expression of *Tgfb1*, *Mcp1*, and *Il33* inflammatory and fibrosis-related genes, whereas ECM hydrogel does not, affirming its biocompatibility. Such a reduced inflammatory response from ECM hydrogel minimizes fibrotic complications, highlighting, in agreement with previous studies (*63*–*65*), divergent immune microenvironments induced by synthetic and biologic materials. Despite the fact that the ECM hydrogel is porcine bone derived, it does not induce an immune rejection response but acts as an anti-inflammatory substrate for several reasons, primarily related to its immunogenicity. The ECM hydrogel is created through a decellularization process that removes cellular components, which are typically responsible for eliciting an antigenic immune response (*66*). This process leaves behind the ECM, which mainly consists of structural proteins such as collagens that are highly conserved across species. Second, it is well established that ECM-based hydrogels can create a proregenerative environment. Studies have shown that ECM materials can promote a shift from a proinflammatory (M1) macrophage phenotype to an anti-inflammatory (M2) phenotype. This shift is crucial for tissue repair and regeneration given that M2 macrophages secrete anti-inflammatory cytokines and growth factors that facilitate healing (*35*, *63*).

Last, the ECM hydrogel was assayed in an alternative preclinical model of development of adhesions, uterine horn abrasion in rabbits (*67*–*69*). ECM hydrogel application was found to diminish adhesions that connect uterine serosal surfaces. In addition, the lack of evidence of MMT (submesothelial areas double-positive for CK and α-SMA), as well as the lack of inflammation-associated staining (CD45) in the perimetrium zone of uterine horns treated with the ECM hydrogel, as compared with untreated rabbits, reinforces the biological and anti-inflammatory effect observed in mice. The rabbit uterine horn abrasion model recapitulates the formation of PAs that interconnect visceral serosa layers, whereas the IB-based mouse model reproduces PAs that bind the parietal peritoneum to viscera. Therefore, we demonstrate that the ECM hydrogel can interfere with PAs in both visceral and parietal injured serosal layers and in both colorectal and gynecological laparotomy applications.

In general, other tissue protector materials lack longevity at the surgically injured site, and physical barriers, such as films or sheets, are difficult to handle and apply. Our ECM hydrogel obtained through decellularization of bone tissue is thermosensitive and exhibits intermediate solid-liquid properties. Below 22°C, it is a liquid with low viscosity, allowing it to be easily applied as a spray. When it is heated to 30° to 37°C, it quickly forms a gel, allowing it to remain in the administration zone. Because of this viscoelastic behavior, the ECM hydrogel maintains the separation of tissues while enabling the intraperitoneal mobility of the visceral organs. Moreover, the thermogelling is not reversible for the ECM hydrogel, but it is for Pluronic F-127. In contrast with other synthetic materials, the ECM hydrogel does not induce a pronounced foreign body response but acts as a healing substrate. In addition, although Pluronic F-127 acts as a physical barrier, ECM hydrogel mitigated PA formation by acting as a physical barrier with a scaffold immune microenvironment with anti-MMT and immune-modulatory properties. Moreover, pig bone, as a widely available by-product of the meat industry, serves as a cost-effective and accessible raw material for large-scale production. In this regard, established supply chains for medical-grade animal tissues enhance feasibility by enabling reliable procurement. Although the raw material itself is inexpensive, downstream processing, particularly enzymatic digestion, sterilization, and good manufacturing practices (GMP) quality controls, introduces most of the production cost. Ensuring batch-to-batch consistency and regulatory-grade safety adds further expense. Even so, the overall workflow benefits from economies of scale: Unit operations are easily expanded, no recombinant proteins or cell culture is required, and capital equipment is standard to bioprocessing facilities.

This study had limitations that warrant mention. First, the RNA-seq studies were performed after culturing the primary cells on plastic plates, under homogeneous conditions. Although we have previously demonstrated that the phenotype and gene expression of MCs cultured ex vivo are maintained, at least during two or three passages, and are representative of the in vivo situations, more robust upfront assessments of adhesion-derived cells from mouse and human tissues are required. Second, RNA-seq pointed to altered Hippo and caveolar signaling, but we did not measure downstream protein readouts in vivo; ongoing studies will test whether hydrogel treatment restores CAV1 expression and YAP nuclear localization in vitro and in vivo. Third, the data suggested that the conversion of MCs into myofibroblasts is the central event in PA formation, despite other minority populations of fibroblasts that could also contribute to this pathology. Direct lineage tracing experiments would further confirm that the $PDPN^+$ myofibroblasts in PAs share a common origin from MCs. Fourth, the ECM hydrogel was assayed in two preclinical models of PA development that only partially mimic the clinical situation. Future studies should evaluate the effect of the ECM hydrogel in more clinically relevant models, with widespread adhesions in the peritoneal cavity, to determine its feasibility in clinical settings. Fifth, although the dominant benefit of the ECM hydrogel appears to come from the physical barrier, we cannot exclude additional contributions from cytokine sorption or integrin-mediated signaling by the ECM scaffold, which will require focused mechanistic work.

In summary, the prophylactic effect of the ECM hydrogel, together with its biocompatibility, makes it an ideal biomaterial for further study in clinical trials. This therapeutic strategy could minimize the risk of PA formation after abdominal surgery and may also be useful in other interventions that can yield fibrogenesis at intraperitoneal localized sites or other predictable sites, such as in surgeries for the insertion of peritoneal dialysis catheters. Therefore, our ECM hydrogel could find wide utility for surgical procedures where the use of current physical barriers is contraindicated, such as those that involve resection of part of the intestine and subsequent intestinal reconnection (anastomosis), which are mainly related to colorectal cancer, intestinal obstruction, or inflammatory bowel diseases (*70*–*76*). Previous preclinical and clinical studies have shown that ECM components can reduce morbidity by promoting intestinal healing in cases of anastomosis (*77*–*80*).

MATERIALS AND METHODS

Study design

The objective of this study was to investigate whether an ECM hydrogel has a protective role in the formation of postsurgical PAs. A further objective assessed by RNA-seq is whether a PA mouse model reflects the MMT-related changes that are observed in patients. In vitro experiments assessed the effect of ECM hydrogel on the MMT process induced by mechanical stretch stimuli. In the human RNA-seq study, four HPMC samples and three HPAMCs were used. In the mouse RNA-seq study, four samples were used per group. Primary MC cultures were expanded before use to obtain sufficient material for RNA-seq studies and further in vitro experiments. In vitro experiments were repeated at least three times per duplicate to ensure statistical power. In mouse treatment studies, each experiment used eight mice per group. In a rabbit uterine horn abrasion model, four animals received treatment, and five were left untreated. There were no dropouts due to morbidity, animals were randomly grouped, and blinding was performed.

Patient biopsies

This study complies with the Declaration of Helsinki and was approved by the Research Ethics Committee of Hospital Universitario La Princesa (Madrid, Spain; ethics approval number: CEIm 21/22). Informed written consent to use biological samples was obtained from patients. A total of three PA biopsies were obtained from patients undergoing abdominal surgery (one each from one patient). Tissue samples were fixed with neutral buffered formalin for 24 hours and processed routinely for immunohistochemical analysis.

Primary patient cells

Primary HPMCs were obtained from omentum samples taken from patients undergoing unrelated abdominal surgery, as previously described (*16*). For isolation of HPMCs, omentum tissue samples ($n = 4$) were digested with a 0.125% trypsin solution containing 0.01% EDTA for 10 min with occasional agitation at 37°C. Cells were cultured in Earle's M199 medium (Biological Industries) supplemented with 20% fetal bovine serum (FBS; Thermo Fisher Scientific) and 2% Biogro-2 (Biological Industries), at 37°C and 5% CO_2. HPMCs were grown to confluence and remained stable for at least two passages before use.

Primary HPAMCs were obtained from ex vivo culture of postsurgical PA samples. For isolation of HPAMCs, postsurgical PA tissue samples ($n = 3$) were cut into small pieces of ~2 to 3 mm^3. Explants were cultured in high cell bind culture plates (25-cm^2 flask; Corning) in Earle's M199 medium (Biological Industries) supplemented with 20% FBS (Thermo Fisher Scientific) and 2% Biogro-2 (Biological Industries) at 37°C and 5% CO_2 to 75% confluency. The remaining tissue pieces were removed, and attached cells were grown to confluence. According to previous studies (*16*, *39*, *46*, *55*, *79*), both morphology and gene expression of MCs remained stable for at least two passages before use.

Primary mouse cells

Primary MPMCs were obtained from the peritoneal cavities of four C57BL/6J mice (Charles River Laboratories). Primary MPAMCs were isolated from ex vivo culture of small pieces of tissue obtained from PAs formed in a total of four mice undergoing an IB-based surgery model. The experimental protocol followed the National Institutes of Health Guide for Care and Use of Laboratory Animals and was approved by the Community of Madrid (Spain; PROEX number 273/19). See Supplementary Materials and Methods for details.

Procedures for cell sorting [fluorescence-activated cell sorting (FACS), RNA-seq, ECM hydrogel preparation, tissue adherence of ECM hydrogel and Pluronic F-127, ECM hydrogel proteomic, mechanical cyclic stretching, RT-qPCR, mouse PA model, in vivo retention study, rabbit uterine horn abrasion model, immunohistochemistry, and dual-immunofluorescence staining] are described in Supplementary Materials and Methods. PAs in mice were quantified following table S1. Specific human and mouse primers used for RT-qPCR studies are listed in tables S2 and S3, respectively. Preoperative and postoperative medications provided to rabbits undergoing surgery are described in tables S4 and S5, respectively. PAs in rabbits were scored for area and strength as described in tables S6 and S7, respectively. ECM hydrogel proteomic raw data are available in data file S2.

Statistical analysis

All statistical analyses were carried out with GraphPad Prism V.8.0.1 (GraphPad Software). The data were compared with two-tailed *t* test (only two groups compared) for Fig. 2D. Statistical significance was determined using Kruskal-Wallis test with post hoc nonparametric (Shapiro-Wilks test) Mann-Whitney rank-sum *U* test in Figs. 3, 5, 6, and 7. The data were compared with nonparametric (Shapiro-Wilks test) Mann-Whitney rank-sum *U* test in Fig. 8. Sample sizes are noted in the figure legends. $P < 0.05$ was considered statistically significant in all cases. All individual-level tabular data are available in data file S3.

Supplementary Materials

The PDF file includes:

Materials and Methods
Figs. S1 to S10
Tables S1 to S7

Other Supplementary Material for this manuscript includes the following:

Data files S1 to S3
MDAR Reproducibility Checklist

REFERENCES AND NOTES

1. D. S. Foster, C. D. Marshall, G. S. Gulati, M. S. Chinta, A. Nguyen, A. Salhotra, R. E. Jones, A. Burcham, T. Lerbs, L. Cui, M. E. King, A. L. Titan, R. C. Ransom, A. Manjunath, M. S. Hu, C. P. Blackshear, S. Mascharak, A. L. Moore, J. A. Norton, C. J. Kin, A. A. Shelton, M. Januszyk, G. C. Gurtner, G. Wernig, M. T. Longaker, Elucidating the fundamental fibrotic processes driving abdominal adhesion formation. *Nat. Commun.* **11**, 4061 (2020).
2. A. N. Imudia, S. Kumar, G. M. Saed, M. P. Diamond, Pathogenesis of Intra-abdominal and pelvic adhesion development. *Semin. Reprod. Med.* **26**, 289–297 (2008).
3. T. Liakakos, N. Thomakos, P. M. Fine, C. Dervenis, R. L. Young, Peritoneal adhesions: Etiology, pathophysiology, and clinical significance. Recent advances in prevention and management. *Dig. Surg.* **18**, 260–273 (2001).
4. B. Schnuriger, G. Barmparas, B. C. Branco, T. Lustenberger, K. Inaba, D. Demetriades, Prevention of postoperative peritoneal adhesions: A review of the literature. *Am. J. Surg.* **201**, 111–121 (2011).
5. M. Canis, R. Botchorishvili, N. Bourdel, A. S. Gremeau, S. Curinier, B. Rabischong, Pelvic adhesions and fertility: Where are we in 2018? *J. Visc. Surg.* **155** (Suppl. 1), S11–S15 (2018).
6. W. Arung, M. Meurisse, O. Detry, Pathophysiology and prevention of postoperative peritoneal adhesions. *World J. Gastroenterol.* **17**, 4545–4553 (2011).
7. D. Moris, J. Chakedis, A. A. Rahnemai-Azar, A. Wilson, M. M. Hennessy, A. Athanasiou, E. W. Beal, C. Argyrou, E. Felekouras, T. M. Pawlik, Postoperative abdominal adhesions: Clinical significance and advances in prevention and management. *J. Gastrointest. Surg.* **21**, 1713–1722 (2017).
8. S. E. Herrick, J. E. Allen, Surgical adhesions: A sticky macrophage problem. *Science* **371**, 993–994 (2021).
9. Q. Hu, X. Xia, X. Kang, P. Song, Z. Liu, M. Wang, X. Lu, W. Guan, S. Liu, A review of physiological and cellular mechanisms underlying fibrotic postoperative adhesion. *Int. J. Biol. Sci.* **17**, 298–306 (2021).
10. S. E. Herrick, B. Wilm, Post-surgical peritoneal scarring and key molecular mechanisms. *Biomolecules* **11**, 692 (2021).

11. N. Di Paolo, G. Sacchi, Atlas of peritoneal histology. *Perit. Dial. Int.* **20** (Suppl. 3), S5–96 (2000).
12. S. E. Mutsaers, The mesothelial cell. *Int. J. Biochem. Cell Biol.* **36**, 9–16 (2004).
13. J. O. van Baal, K. K. Van de Vijver, R. Nieuwland, C. J. van Noorden, W. J. van Driel, A. Sturk, G. G. Kenter, L. G. Rikkert, C. A. Lok, The histophysiology and pathophysiology of the peritoneum. *Tissue Cell* **49**, 95–105 (2017).
14. P. Sandoval, J. A. Jimenez-Heffernan, G. Guerra-Azcona, M. L. Perez-Lozano, A. Rynne-Vidal, P. Albar-Vizcaino, F. Gil-Vera, P. Martin, M. J. Coronado, C. Barcena, J. Dotor, P. L. Majano, A. A. Peralta, M. Lopez-Cabrera, Mesothelial-to-mesenchymal transition in the pathogenesis of post-surgical peritoneal adhesions. *J. Pathol.* **239**, 48–59 (2016).
15. R. Kalluri, R. A. Weinberg, The basics of epithelial-mesenchymal transition. *J. Clin. Invest.* **119**, 1420–1428 (2009).
16. M. Yanez-Mo, E. Lara-Pezzi, R. Selgas, M. Ramirez-Huesca, C. Dominguez-Jimenez, J. A. Jimenez-Heffernan, A. Aguilera, J. A. Sanchez-Tomero, M. A. Bajo, V. Alvarez, M. A. Castro, G. del Peso, A. Cirujeda, C. Gamallo, F. Sanchez-Madrid, M. Lopez-Cabrera, Peritoneal dialysis and epithelial-to-mesenchymal transition of mesothelial cells. *N. Engl. J. Med.* **348**, 403–413 (2003).
17. L. S. Aroeira, A. Aguilera, J. A. Sanchez-Tomero, M. A. Bajo, G. del Peso, J. A. Jimenez-Heffernan, R. Selgas, M. Lopez-Cabrera, Epithelial to mesenchymal transition and peritoneal membrane failure in peritoneal dialysis patients: Pathologic significance and potential therapeutic interventions. *J. Am. Soc. Nephrol.* **18**, 2004–2013 (2007).
18. M. López-Cabrera, Mesenchymal conversion of mesothelial cells is a key event in the pathophysiology of the peritoneum during peritoneal dialysis. *Adv. Med.* **2014**, 473134 (2014).
19. A. Hanna, Y. Pang, C. W. Bedrossian, A. Dejmek, C. W. Michael, Podoplanin is a useful marker for identifying mesothelioma in malignant effusions. *Diagn. Cytopathol.* **38**, 264–269 (2010).
20. J. M. Tsai, R. Sinha, J. Seita, N. Fernhoff, S. Christ, T. Koopmans, G. W. Krampitz, K. M. McKenna, L. Xing, M. Sandholzer, J. H. Sales, M. Shoham, M. McCracken, L. M. Joubert, S. R. Gordon, N. Poux, G. Wernig, J. A. Norton, I. L. Weissman, Y. Rinkevich, Surgical adhesions in mice are derived from mesothelial cells and can be targeted by antibodies against mesothelial markers. *Sci. Transl. Med.* **10**, eaan6735 (2018).
21. R. Strippoli, P. Sandoval, R. Moreno-Vicente, L. Rossi, C. Battistelli, M. Terri, L. Pascual-Anton, M. Loureiro, F. Matteini, E. Calvo, J. A. Jimenez-Heffernan, M. J. Gomez, V. Jimenez-Jimenez, F. Sanchez-Cabo, J. Vazquez, M. Tripodi, M. Lopez-Cabrera, M. A. Del Pozo, Caveolin1 and YAP drive mechanically induced mesothelial to mesenchymal transition and fibrosis. *Cell Death Dis.* **11**, 647 (2020).
22. R. Strippoli, J. Loureiro, V. Moreno, I. Benedicto, M. L. Lozano, O. Barreiro, T. Pellinen, S. Minguet, M. Foronda, M. T. Osteso, E. Calvo, J. Vazquez, M. L. Cabrera, M. A. Del Pozo, Caveolin-1 deficiency induces a MEK-ERK1/2-Snail-1-dependent epithelial-mesenchymal transition and fibrosis during peritoneal dialysis. *EMBO Mol. Med.* **7**, 102–123 (2015).
23. J. Tang, Z. Xiang, M. T. Bernards, S. Chen, Peritoneal adhesions: Occurrence, prevention and experimental models. *Acta Biomater.* **116**, 84–104 (2020).
24. S. H. Oh, J. K. Kim, K. S. Song, S. M. Noh, S. H. Ghil, S. H. Yuk, J. H. Lee, Prevention of postsurgical tissue adhesion by anti-inflammatory drug-loaded pluronic mixtures with sol-gel transition behavior. *J. Biomed. Mater. Res. A* **72**, 306–316 (2005).
25. J. Liao, X. Li, Y. Fan, Prevention strategies of postoperative adhesion in soft tissues by applying biomaterials: Based on the mechanisms of occurrence and development of adhesions. *Bioact. Mater.* **26**, 387–412 (2023).
26. A. K. S. Chandel, A. Shimizu, K. Hasegawa, T. Ito, Advancement of biomaterial-based postoperative adhesion barriers. *Macromol. Biosci.* **21**, e2000395 (2021).
27. A. K. Greene, I. P. Alwayn, V. Nose, E. Flynn, D. Sampson, D. Zurakowski, J. Folkman, M. Puder, Prevention of intra-abdominal adhesions using the antiangiogenic COX-2 inhibitor celecoxib. *Ann. Surg.* **242**, 140–146 (2005).
28. L. Song, L. Li, T. He, N. Wang, S. Yang, X. Yang, Y. Zeng, W. Zhang, L. Yang, Q. Wu, C. Gong, Peritoneal adhesion prevention with a biodegradable and injectable N,O-carboxymethyl chitosan-aldehyde hyaluronic acid hydrogel in a rat repeated-injury model. *Sci. Rep.* **6**, 37600 (2016).
29. R. P. G. Ten Broek, M. W. J. Stommel, C. Strik, C. van Laarhoven, F. Keus, H. van Goor, Benefits and harms of adhesion barriers for abdominal surgery: A systematic review and meta-analysis. *Lancet* **383**, 48–59 (2014).
30. P. Krielen, J. P. C. Grutters, C. Strik, R. P. G. Ten Broek, H. van Goor, M. W. J. Stommel, Cost-effectiveness of the prevention of adhesions and adhesive small bowel obstruction after colorectal surgery with adhesion barriers: A modelling study. *World J. Emerg. Surg.* **14**, 41 (2019).
31. J. Zindel, M. Peiseler, M. Hossain, C. Deppermann, W. Y. Lee, B. Haenni, B. Zuber, J. F. Deniset, B. G. J. Surewaard, D. Candinas, P. Kubes, Primordial GATA6 macrophages function as extravascular platelets in sterile injury. *Science* **371**, eabe0595 (2021).
32. G. Wei, Z. Wang, R. Liu, C. Zhou, E. Li, T. Shen, X. Wang, Y. Wu, X. Li, A combination of hybrid polydopamine-human keratinocyte growth factor nanoparticles and sodium hyaluronate for the efficient prevention of postoperative abdominal adhesion formation. *Acta Biomater.* **138**, 155–167 (2022).
33. M. Fujita, G. M. Policastro, A. Burdick, H. T. Lam, J. L. Ungerleider, R. L. Braden, D. Huang, K. G. Osborn, J. H. Omens, M. M. Madani, K. L. Christman, Preventing post-surgical cardiac adhesions with a catechol-functionalized oxime hydrogel. *Nat. Commun.* **12**, 3764 (2021).
34. S. F. Badylak, The extracellular matrix as a biologic scaffold material. *Biomaterials* **28**, 3587–3593 (2007).
35. T. J. Keane, S. F. Badylak, The host response to allogeneic and xenogeneic biological scaffold materials. *J. Tissue Eng. Regen. Med.* **9**, 504–511 (2015).
36. T. D. Johnson, S. Y. Lin, K. L. Christman, Tailoring material properties of a nanofibrous extracellular matrix derived hydrogel. *Nanotechnology* **22**, 494015 (2011).
37. I. Hirahara, H. Sato, T. Imai, A. Onishi, Y. Morishita, S. Muto, E. Kusano, D. Nagata, Methylglyoxal induced basophilic spindle cells with podoplanin at the surface of peritoneum in rat peritoneal dialysis model. *Biomed. Res. Int.* **2015**, 289751 (2015).
38. N. Braun, D. M. Alscher, P. Fritz, I. Edenhofer, M. Kimmel, A. Gaspert, F. Reimold, B. Bode-Lesniewska, U. Ziegler, D. Biegger, R. P. Wuthrich, S. Segerer, Podoplanin-positive cells are a hallmark of encapsulating peritoneal sclerosis. *Nephrol. Dial. Transplant.* **26**, 1033–1041 (2011).
39. N. Braun, M. D. Alscher, P. Fritz, J. Latus, I. Edenhofer, F. Reimold, S. L. Alper, M. Kimmel, D. Biegger, M. Lindenmeyer, C. D. Cohen, R. P. Wuthrich, S. Segerer, The spectrum of podoplanin expression in encapsulating peritoneal sclerosis. *PLOS ONE* **7**, e53382 (2012).
40. L. Pascual-Anton, P. Sandoval, G. T. Gonzalez-Mateo, V. Kopytina, H. Tomero-Sanz, E. M. Arriero-Pais, J. A. Jimenez-Heffernan, M. Fabre, I. Egana, C. Ferrer, L. Simon, L. Gonzalez-Cortijo, R. Sainz de la Cuesta, M. Lopez-Cabrera, Targeting carcinoma-associated mesothelial cells with antibody-drug conjugates in ovarian carcinomatosis. *J. Pathol.* **261**, 238–251 (2023).
41. L. M. Stapleton, A. N. Steele, H. Wang, H. Lopez Hernandez, A. C. Yu, M. J. Paulsen, A. A. A. Smith, G. A. Roth, A. D. Thakore, H. J. Lucian, K. P. Totherow, S. W. Baker, Y. Tada, J. M. Farry, A. Eskandari, C. E. Hironaka, K. J. Jaatinen, K. M. Williams, H. Bergamasco, C. Marschel, B. Chadwick, F. Grady, M. Ma, E. A. Appel, Y. J. Woo, Use of a supramolecular polymeric hydrogel as an effective post-operative pericardial adhesion barrier. *Nat. Biomed. Eng.* **3**, 611–620 (2019).
42. N. D. Evans, R. O. Oreffo, E. Healy, P. J. Thurner, Y. H. Man, Epithelial mechanobiology, skin wound healing, and the stem cell niche. *J. Mech. Behav. Biomed. Mater.* **28**, 397–409 (2013).
43. Z. Li, L. Liu, Y. Chen, Dual dynamically crosslinked thermosensitive hydrogel with self-fixing as a postoperative anti-adhesion barrier. *Acta Biomater.* **110**, 119–128 (2020).
44. Y. Wang, W. Zhai, L. Yang, S. Cheng, W. Cui, J. Li, Establishments and evaluations of post-operative adhesion animal models. *Adv. Ther.* **6**, 2200297 (2023).
45. M. Mack, Inflammation and fibrosis. *Matrix Biol.* **68-69**, 106–121 (2018).
46. S. A. Ricketts, P. D. Sibbons, C. J. Green, Quantitative analysis of the development of experimentally induced post surgical adhesions: A microstereological study. *Int. J. Exp. Pathol.* **80**, 325–334 (1999).
47. A. Rynne-Vidal, C. L. Au-Yeung, J. A. Jimenez-Heffernan, M. L. Perez-Lozano, L. Cremades-Jimeno, C. Barcena, I. Cristobal-Garcia, C. Fernandez-Chacon, T. L. Yeung, S. C. Mok, P. Sandoval, M. Lopez-Cabrera, Mesothelial-to-mesenchymal transition as a possible therapeutic target in peritoneal metastasis of ovarian cancer. *J. Pathol.* **242**, 140–151 (2017).
48. J. Loureiro, A. Aguilera, R. Selgas, P. Sandoval, P. Albar-Vizcaino, M. L. Perez-Lozano, V. Ruiz-Carpio, P. L. Majano, S. Lamas, F. Rodriguez-Pascual, F. Borras-Cuesta, J. Dotor, M. Lopez-Cabrera, Blocking TGF-beta1 protects the peritoneal membrane from dialysate-induced damage. *J. Am. Soc. Nephrol.* **22**, 1682–1695 (2011).
49. M. J. Strowitzki, A. S. Ritter, G. Kimmer, M. Schneider, Hypoxia-adaptive pathways: A pharmacological target in fibrotic disease? *Pharmacol. Res.* **147**, 104364 (2019).
50. E. L. Shelton, C. L. Galindo, C. H. Williams, E. Pfaltzgraff, C. C. Hong, D. M. Bader, Autotaxin signaling governs phenotypic heterogeneity in visceral and parietal mesothelia. *PLOS ONE* **8**, e69712 (2013).
51. K. Kawanishi, Diverse properties of the mesothelial cells in health and disease. *Pleura Peritoneum* **1**, 79–89 (2016).
52. S. Namvar, A. S. Woolf, L. A. Zeef, T. Wilm, B. Wilm, S. E. Herrick, Functional molecules in mesothelial-to-mesenchymal transition revealed by transcriptome analyses. *J. Pathol.* **245**, 491–501 (2018).
53. J. Chen, X. Tang, Z. Wang, A. Perez, B. Yao, K. Huang, Y. Zhang, M. W. King, Techniques for navigating postsurgical adhesions: Insights into mechanisms and future directions. *Bioeng. Transl. Med.* **8**, e10565 (2023).
54. J. Gao, J. Wen, D. Hu, K. Liu, Y. Zhang, X. Zhao, K. Wang, Bottlebrush inspired injectable hydrogel for rapid prevention of postoperative and recurrent adhesion. *Bioact. Mater.* **16**, 27–46 (2022).
55. C. Brochhausen, V. H. Schmitt, C. N. Planck, T. K. Rajab, D. Hollemann, C. Tapprich, B. Kramer, C. Wallwiener, H. Hierlemann, R. Zehbe, H. Planck, C. J. Kirkpatrick, Current strategies and future perspectives for intraperitoneal adhesion prevention. *J. Gastrointest. Surg.* **16**, 1256–1274 (2012).

56. M. Zeisberg, E. G. Neilson, Biomarkers for epithelial-mesenchymal transitions. *J. Clin. Invest.* **119**, 1429–1437 (2009).
57. V. Ruiz-Carpio, P. Sandoval, A. Aguilera, P. Albar-Vizcaíno, M. L. Perez-Lozano, G. T. González-Mateo, A. Acuña-Ruiz, J. García-Cantalejo, P. Botías, M. A. Bajo, R. Selgas, J. A. Sánchez-Tomero, J. Passlick-Deetjen, D. Piecha, J. Büchel, S. Steppan, M. López-Cabrera, Genomic reprograming analysis of the mesothelial to mesenchymal transition identifies biomarkers in peritoneal dialysis patients. *Sci. Rep.* **7**, 44941 (2017).
58. S. H. Phan, Biology of fibroblasts and myofibroblasts. *Proc. Am. Thorac. Soc.* **5**, 334–337 (2008).
59. R. B. Diller, A. J. Tabor, The role of the extracellular matrix (ECM) in wound healing: A review. *Biomimetics* **7**, 87 (2022).
60. C. M. Horejs, J. P. St-Pierre, J. R. M. Ojala, J. A. M. Steele, P. B. da Silva, A. Rynne-Vidal, S. A. Maynard, C. S. Hansel, C. Rodriguez-Fernandez, M. M. Mazo, A. Y. F. You, A. J. Wang, T. von Erlach, K. Tryggvason, M. Lopez-Cabrera, M. M. Stevens, Preventing tissue fibrosis by local biomaterials interfacing of specific cryptic extracellular matrix information. *Nat. Commun.* **8**, 15509 (2017).
61. S. F. Badylak, A scaffold immune microenvironment. *Science* **352**, 298 (2016).
62. R. Strippoli, I. Benedicto, M. L. Perez Lozano, A. Cerezo, M. Lopez-Cabrera, M. A. del Pozo, Epithelial-to-mesenchymal transition of peritoneal mesothelial cells is regulated by an ERK/NF-kappaB/Snail1 pathway. *Dis. Model. Mech.* **1**, 264–274 (2008).
63. K. Sadtler, B. W. Allen, K. Estrellas, F. Housseau, D. M. Pardoll, J. H. Elisseeff, The scaffold immune microenvironment: Biomaterial-mediated immune polarization in traumatic and nontraumatic applications. *Tissue Eng. Part A* **23**, 1044–1053 (2017).
64. K. Sadtler, K. Estrellas, B. W. Allen, M. T. Wolf, H. Fan, A. J. Tam, C. H. Patel, B. S. Luber, H. Wang, K. R. Wagner, J. D. Powell, F. Housseau, D. M. Pardoll, J. H. Elisseeff, Developing a pro-regenerative biomaterial scaffold microenvironment requires T helper 2 cells. *Science* **352**, 366–370 (2016).
65. K. Sadtler, M. T. Wolf, S. Ganguly, C. A. Moad, L. Chung, S. Majumdar, F. Housseau, D. M. Pardoll, J. H. Elisseeff, Divergent immune responses to synthetic and biological scaffolds. *Biomaterials* **192**, 405–415 (2019).
66. M. J. Sawkins, W. Bowen, P. Dhadda, H. Markides, L. E. Sidney, A. J. Taylor, F. R. Rose, S. F. Badylak, K. M. Shakesheff, L. J. White, Hydrogels derived from demineralized and decellularized bone extracellular matrix. *Acta Biomater.* **9**, 7865–7873 (2013).
67. R. Dunn, M. D. Lyman, P. G. Edelman, P. K. Campbell, Evaluation of the SprayGel adhesion barrier in the rat cecum abrasion and rabbit uterine horn adhesion models. *Fertil. Steril.* **75**, 411–416 (2001).
68. R. E. Leach, J. W. Burns, E. J. Dawe, M. D. SmithBarbour, M. P. Diamond, Reduction of postsurgical adhesion formation in the rabbit uterine horn model with use of hyaluronate/carboxymethylcellulose gel. *Fertil. Steril.* **69**, 415–418 (1998).
69. D. M. Wiseman, P. Gravagna, Y. Bayon, J. Tayot, Collagen membrane/fleece composite film reduces adhesions in the presence of bleeding in a rabbit uterine horn model. *Fertil. Steril.* **76**, 175–180 (2001).
70. D. E. Beck, Z. Cohen, J. W. Fleshman, H. S. Kaufman, H. van Goor, B. G. Wolff, Adhesion Study Group Steering Committee, A prospective, randomized, multicenter, controlled study of the safety of Seprafilm adhesion barrier in abdominopelvic surgery of the intestine. *Dis. Colon Rectum* **46**, 1310–1319 (2003).
71. W. G. Cheadle, Risk factors for surgical site infection. *Surg. Infect. (Larchmt.)* **7** (Suppl. 1), S7–S11 (2006).
72. M. A. Boccola, P. G. Buettner, W. M. Rozen, S. K. Siu, A. R. Stevenson, R. Stitz, Y.-H. Ho, Risk factors and outcomes for anastomotic leakage in colorectal surgery: A single-institution analysis of 1576 patients. *World J. Surg.* **35**, 186–195 (2011).
73. M. A. Boccola, A. Sharma, C. Taylor, L. M. Wong, D. Travis, S. Chan, The infusion method trial of void vs standard catheter removal in the outpatient setting: A prospective randomized trial. *BJU Int.* **107** (Suppl. 3), 43–46 (2011).
74. A. Mirnezami, R. Mirnezami, K. Chandrakumaran, K. Sasapu, P. Sagar, P. Finan, Increased local recurrence and reduced survival from colorectal cancer following anastomotic leak: Systematic review and meta-analysis. *Ann. Surg.* **253**, 890–899 (2011).
75. C. L. Tang, D. G. Jayne, F. Seow-Choen, Y. Y. Ng, K. W. Eu, N. Mustapha, A randomized controlled trial of 0.5% ferric hyaluronate gel (Intergel) in the prevention of adhesions following abdominal surgery. *Ann. Surg.* **243**, 449–455 (2006).
76. S. Goto, S. Hasegawa, K. Hida, R. Uozumi, Y. Kanemitsu, T. Watanabe, K. Sugihara, Y. Sakai, Study Group for Nomogram of the Japanese Society for Cancer of the Colon and Rectum, Multicenter analysis of impact of anastomotic leakage on long-term oncologic outcomes after curative resection of colon cancer. *Surgery* **162**, 317–324 (2017).
77. J. Hoeppner, V. Crnogorac, U. T. Hopt, H. F. Weiser, The pig as an experimental model for colonic healing study of leakage and ischemia in colonic anastomosis. *J. Invest. Surg.* **22**, 281–285 (2009).
78. J. Hoeppner, G. Marjanovic, P. Helwig, U. T. Hopt, T. Keck, Extracellular matrices for gastrointestinal surgery: Ex vivo testing and current applications. *World J. Gastroenterol.* **16**, 4031–4038 (2010).
79. J. Hoeppner, B. Wassmuth, G. Marjanovic, S. Timme, U. T. Hopt, T. Keck, Anastomotic sealing by extracellular matrices (ECM) improves healing of colonic anastomoses in the critical early phase. *J. Gastrointest. Surg.* **14**, 977–986 (2010).
80. J. Hoeppner, K. Willa, S. Timme, D. Tittelbach-Helmrich, U. T. Hopt, T. Keck, G. Marjanovic, Reinforcement of colonic anastomoses with a collagenous double-layer matrix extracted from porcine dermis. *Eur. Surg. Res.* **45**, 68–76 (2010).

Acknowledgments

Funding: M.L.-C. acknowledges support from the Spanish Ministry of Science and Innovation/Fondo Europeo de Desarrolo Regional (MICIN/FEDER) (PID2022-142796OB-I00/AEI/10.13039/501100011033) and Marie Sklodowska-Curie Innovative Training Networks-European Training Networks (no. 812699). M.L.-C. has received sponsored research funds from TYBR Health Inc. R.S. acknowledges support from the Ministry for Health of Italy (Ricerca Corrente) linea 2. M.A.P. acknowledges support from the Spanish Ministry of Science, Innovation & Universities (MICIU)/Agencia Estatal de Investigación (AEI)/FEDER (PID2023-146414OB-I00/AEI/10.13039/501100011033). The CNIC is supported by the Instituto de Salud Carlos III (ISCIII), the MICIU, and the Pro CNIC Foundation and is a Severo Ochoa Center of Excellence (CEX2020-001041-S funded by MICIN/AEI/10.13039/501100011033). T.J.K. acknowledges the European Union's Horizon 2020 research and innovation programme under the Marie Skłodowska-Curie Individual European Fellowship (no. 746980). M.M.S. acknowledges support from the UK Regenerative Medicine Platform "Acellular/Smart Materials–3D Architecture" hub (MR/R015651/1). For the purpose of open access, the author(s) has applied a Creative Commons Attribution (CC BY) license to any Author Accepted Manuscript version arising from this submission. **Author contributions:** P.S., M.M.S., and M.L.-C. supervised the research study. L.P.-A., P.S., and T.J.K. designed experiments. L.P.-A. and P.S. performed RNA-seq analysis, surgical techniques in mice, immunohistochemistry, and immunofluorescences. L.P.-A. and H.T.-S. performed RT-qPCR studies. L.P.-A., P.S., and M.T. performed and analyzed in vitro mechanical stretch experiments with suggestions from R.S. and M.A.P. I.G.-S. and C.M.-C. provided human adhesion samples. M.O., V.G., P.A.S., and T.J.K. characterized ECM hydrogel, carried out tissue adherence of ECM hydrogel, and designed experiments in rabbits. P.S. analyzed rabbit tissue samples. L.P.-A. and P.S. performed figures. L.P.-A., P.S., and T.J.K. wrote the original draft manuscript. P.S., M.L.-C., and M.M.S. edited the final version of the manuscript. All authors reviewed the manuscript. **Competing interests:** P.A.S. and T.J.K. are cofounders of TYBR Health Inc., which produces the commercial ECM hydrogel; M.O. and V.G. were employees at TYBR Health Inc. during the work; M.M.S. is an adviser to TYBR Health Inc. and also holds a part-time position at the Karolinska Institute. P.A.S. and T.J.K. are coinventors on patents related to this work, including US11925731B2 ("Sprayable stimuli-responsive micro-hydrogels for adhesion prevention and enhanced tissue healing") and US20230372615A1 ("Systems and methods for delivery of multi-component fluids"). All other authors declare that they have no competing interests. **Data and materials availability:** Data files from the human transcriptome profiling analysis were deposited in the European Genome-Phenome Archive (EGA, EGAS00001005749). Data files from the mouse transcriptome profiling analysis were deposited in the European Nucleotide Archive (ENA, PRJEB48465). All data associated with this study are present in the paper or the Supplementary Materials.

Submitted 5 December 2023
Resubmitted 13 February 2025
Accepted 15 September 2025
Published 8 October 2025
10.1126/scitranslmed.adn3179